The Abdus Salam
International Centre for Theoretical Physics

United Nations
Educational, Scientific and
Cultural Organization

IAEA
International Atomic Energy Agency

2060-22

Advanced School on Non-linear Dynamics and Earthquake Prediction

28 September - 10 October, 2009

Structural relaxation and its relation with non-trivial frictional properties

Eduardo A. Jagla
Centro Atomico Bariloche
Argentina

jagla@cab.cnea.gov.ar

Frictional properties from the structural relaxation mechanism

Eduardo A. Jagla

Bariloche, Argentina

Comisión Nacional
de Energía Atómica,
Argentina

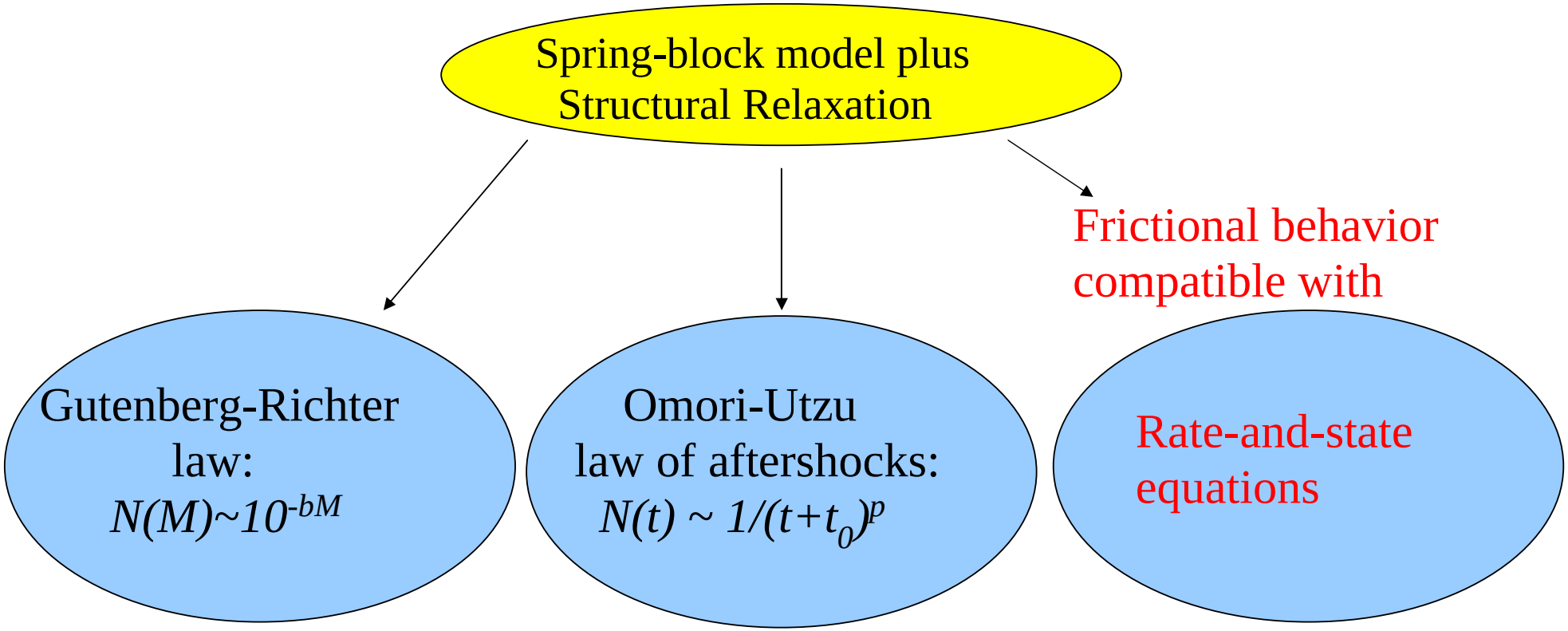
Spring-block model plus
Structural Relaxation
Frictional behavior
compatible with
Gutenberg-Richter
law:
$N(M) \sim 10^{-bM}$
Omori-Utzu
law of aftershocks:
$N(t) \sim 1/(t+t_0)^p$
Rate-and-state
equations

Overview:

- Friction phenomenology

- Rate-and-state equations

- How “structural relaxation” produces non-trivial, realistic friction

Friction phenomenology in geologicaly relevant materials:

-Friction coefficient depends on velocity.

-Friction coefficient *<u>decreases</u>* with velocity (velocity weakening)

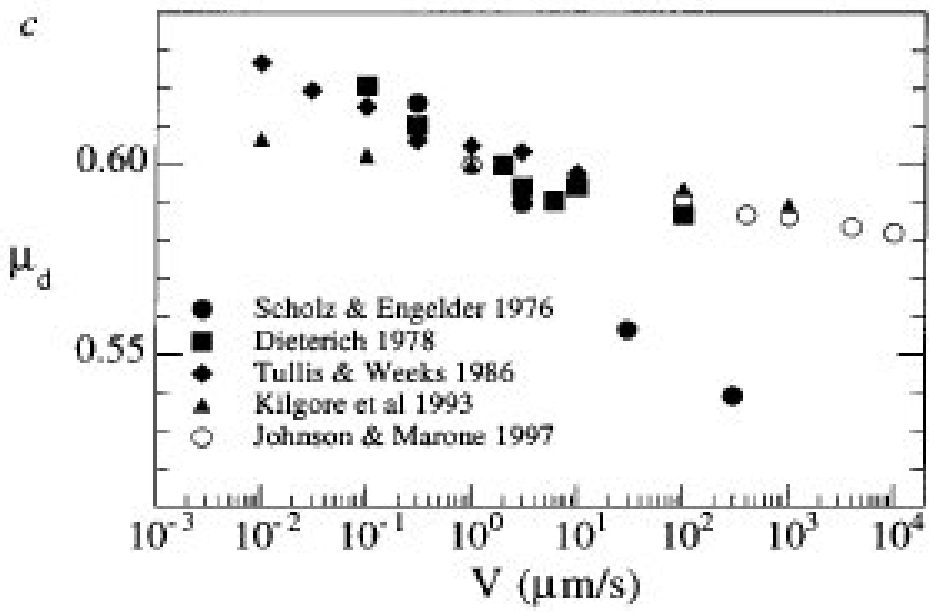

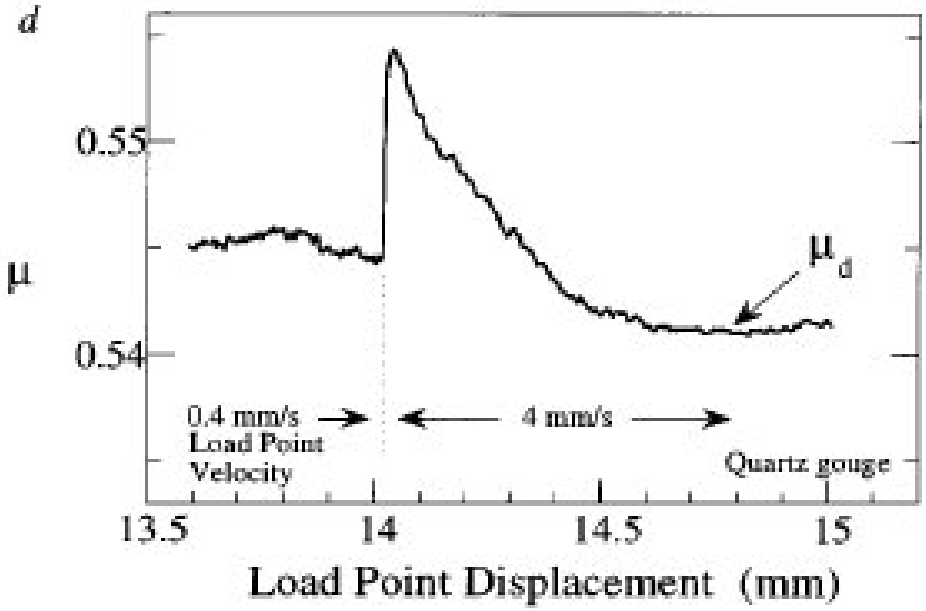

Friction phenomenology in geologicaly relevant materials:

-Friction is history dependent

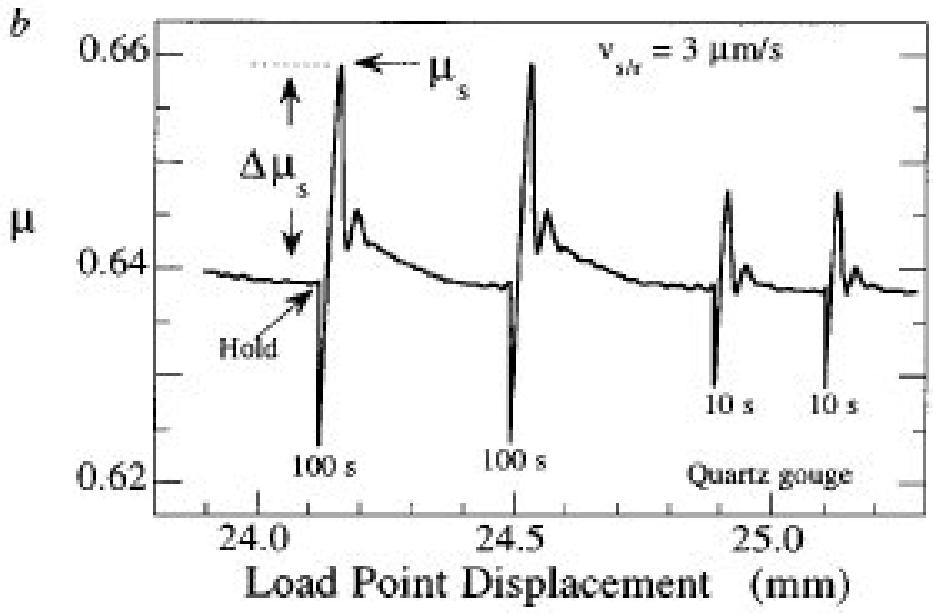

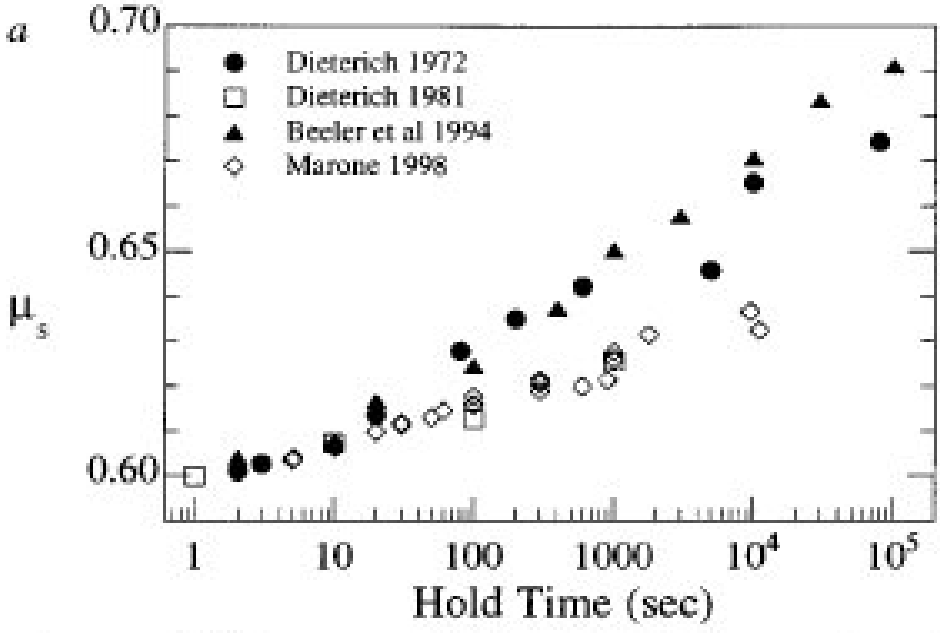

Friction phenomenology in geologicaly relevant materials:

-Phenomenological modeling:
The rate and state equations: Dieterich (1979), Rice&Ruina (1983)

$$\mu = \mu_0 + A\ln(V/V_0) + B\ln(V_0\theta/D_c)$$

$$\frac{d\theta}{dt} = 1 - \frac{\theta V}{D_c} \qquad \theta: \text{ state variable}$$

If $V = 0 \rightarrow \theta = t$

In steady sliding

$$\mu = \mu_0 + (A-B)\ln(V/V_0)$$

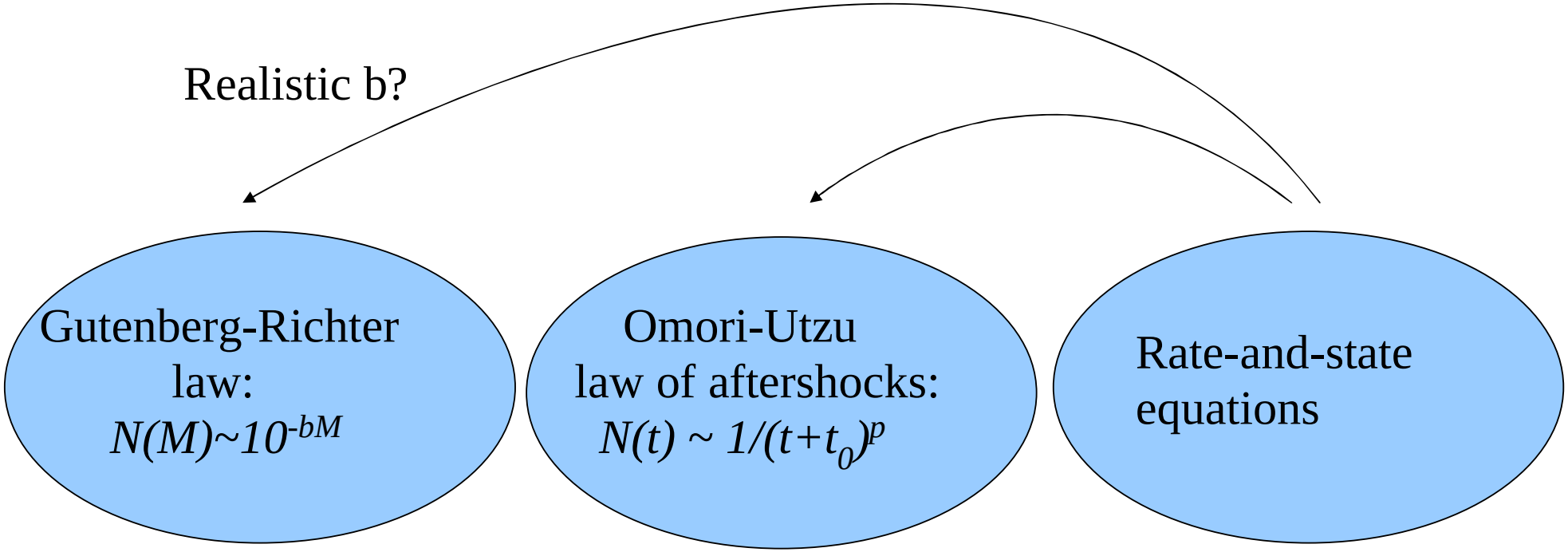

Dieterich (1995)
Ziv and Rubin (2003)

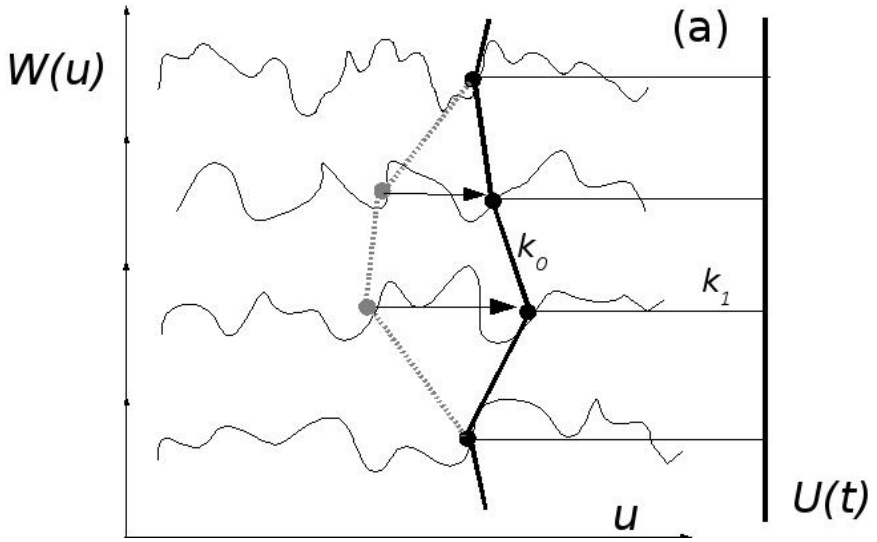

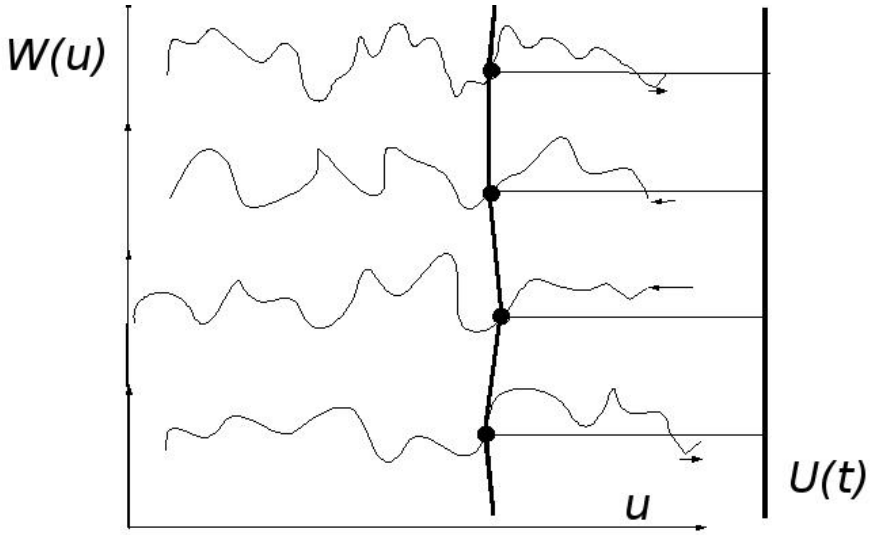

$$E = \sum_{i,j;i',j'} \frac{k_0}{2}(u_{i,j} - u_{i',j'})^2 + \sum_{i,j} \frac{k_1}{2}(U(t) - u_{i,j})^2 + \sum_{i,j} W_{i,j}(u_{i,j})$$

$$\frac{du_{i,j}}{dt} = -\lambda \frac{\delta E}{\delta u_{i,j}}$$

$$\sum_{i,j} W_{i,j}(u_{i,j}) \rightarrow \sum_{i,j} W_{i,j}(u_{i,j} - u^0_{i,j})$$

$$\frac{du^0_{i,j}}{dt} = R\nabla^2 \frac{\delta E}{\delta u^0_{i,j}}$$

k_1 large, viscous sliding

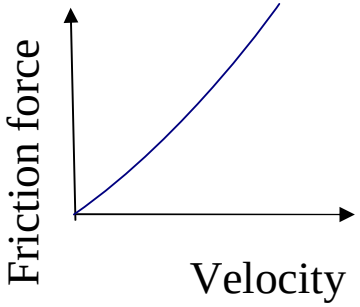

k_1 small, Static friction force

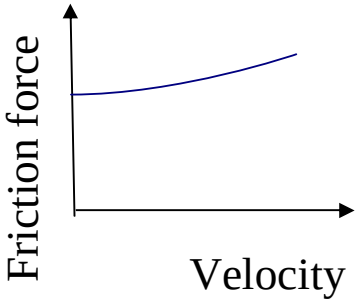

"velocity weakening"

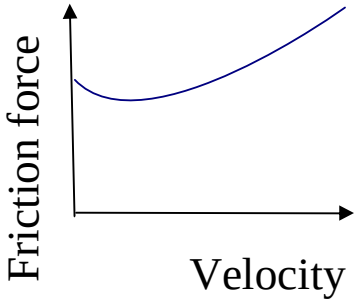

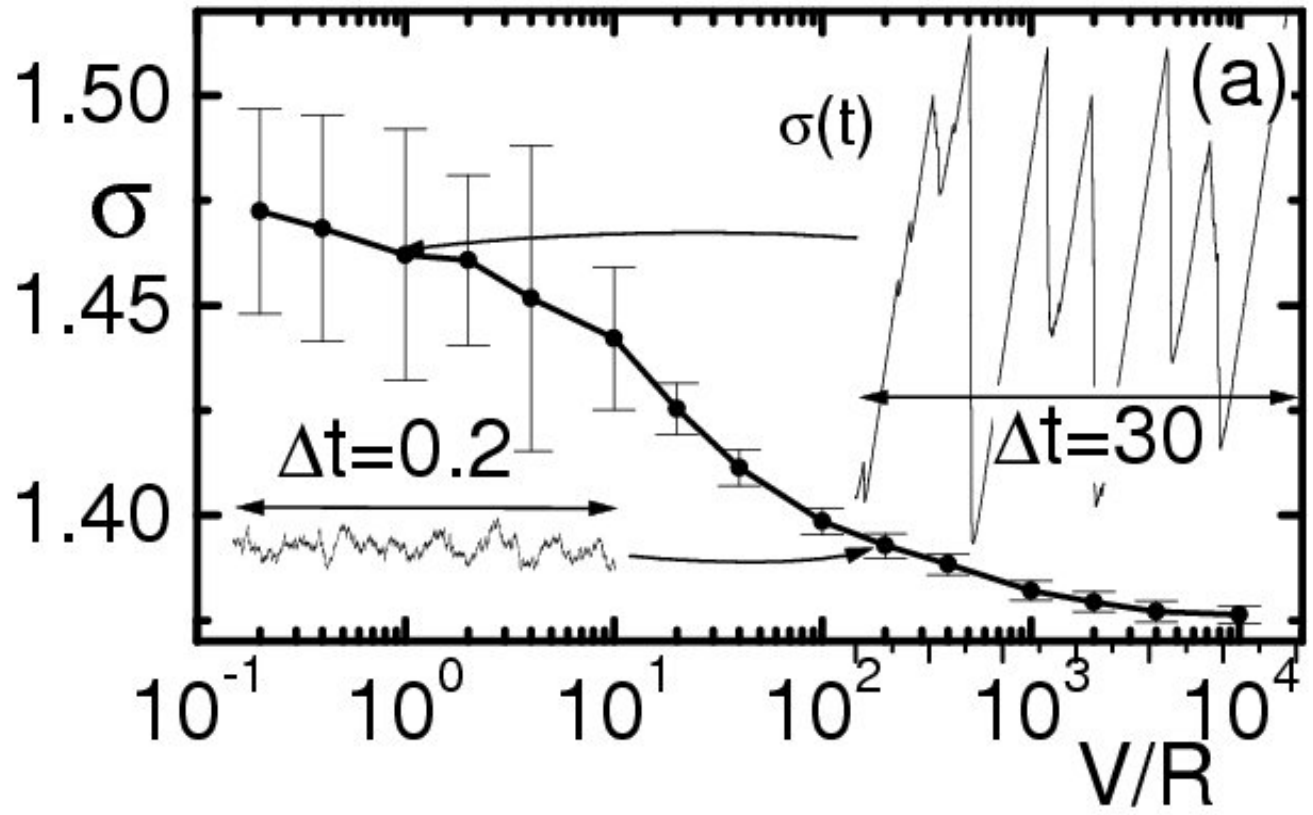
1.50
σ
1.45
1.40
σ(t)
(a)
Δt=0.2
Δt=30
10^-1
10^0
10^1
10^2
10^3
10^4
V/R

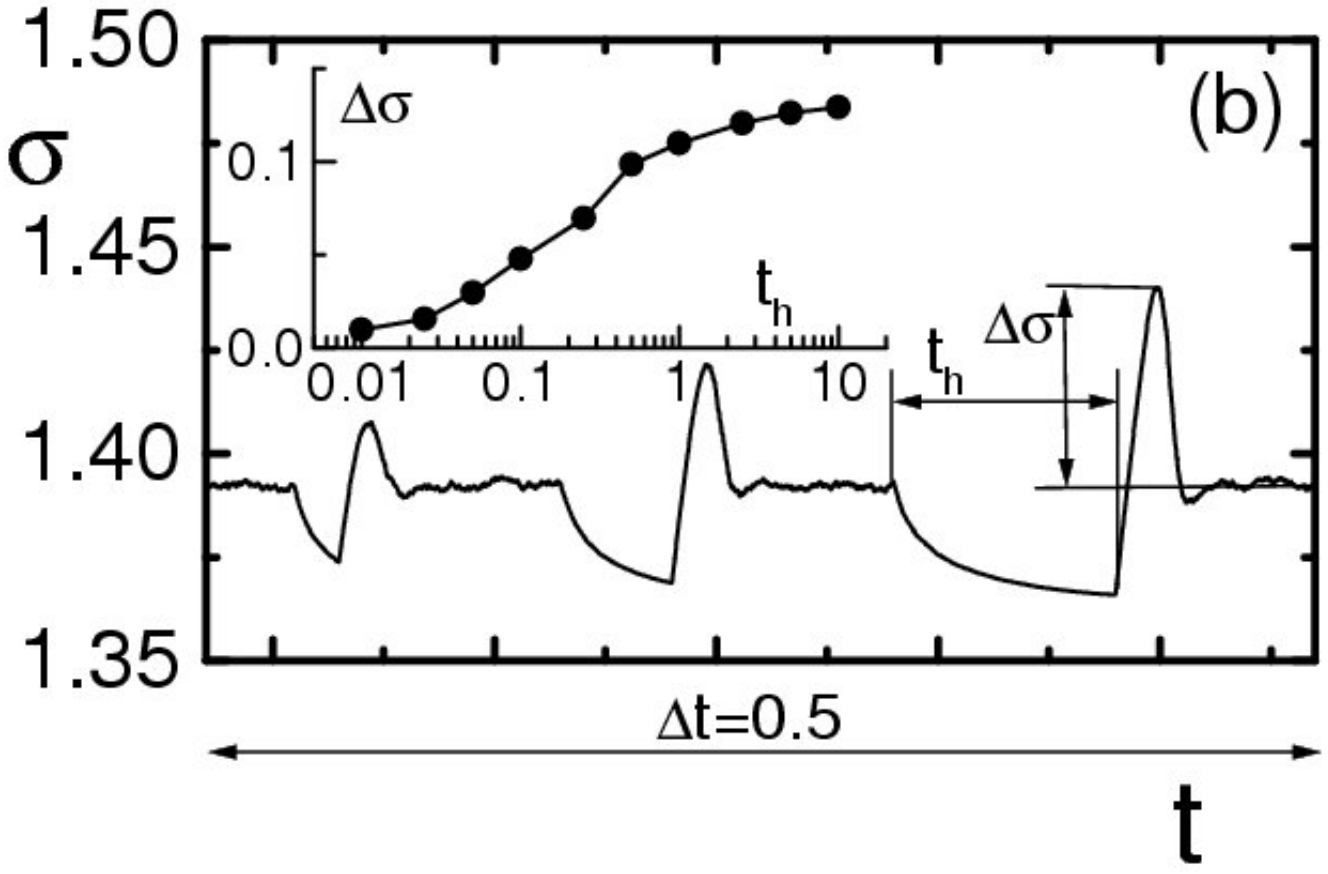
1.50
σ
1.45
1.40
1.35
Δσ
0.1
0.0
0.01
0.1
1
10
t_h
(b)
t_h
Δσ
Δt=0.5
t

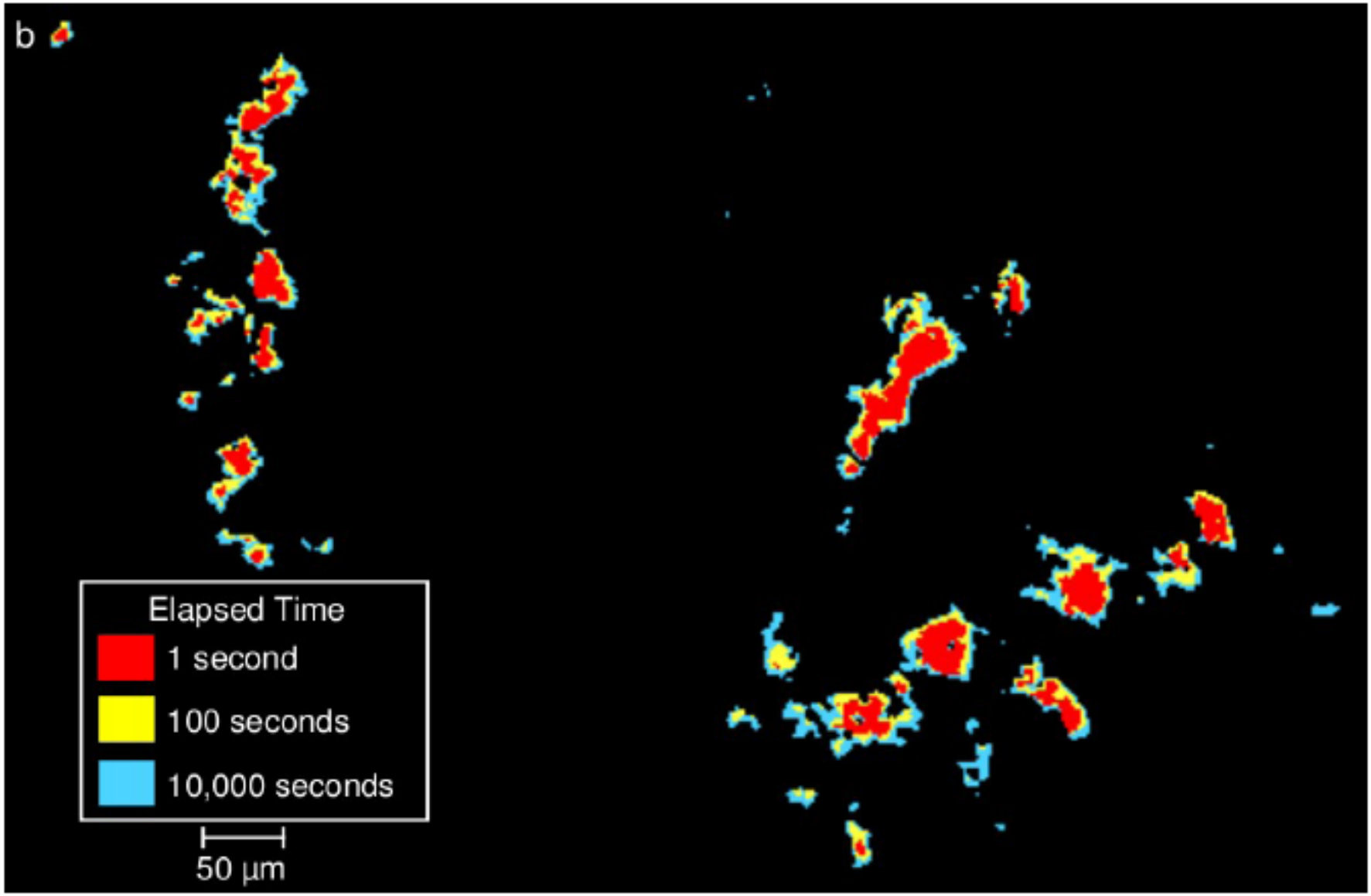

Dieterich and Kilgore, 1994

Is Structural relaxation compatible with time increase of contact area?

Yes, it is

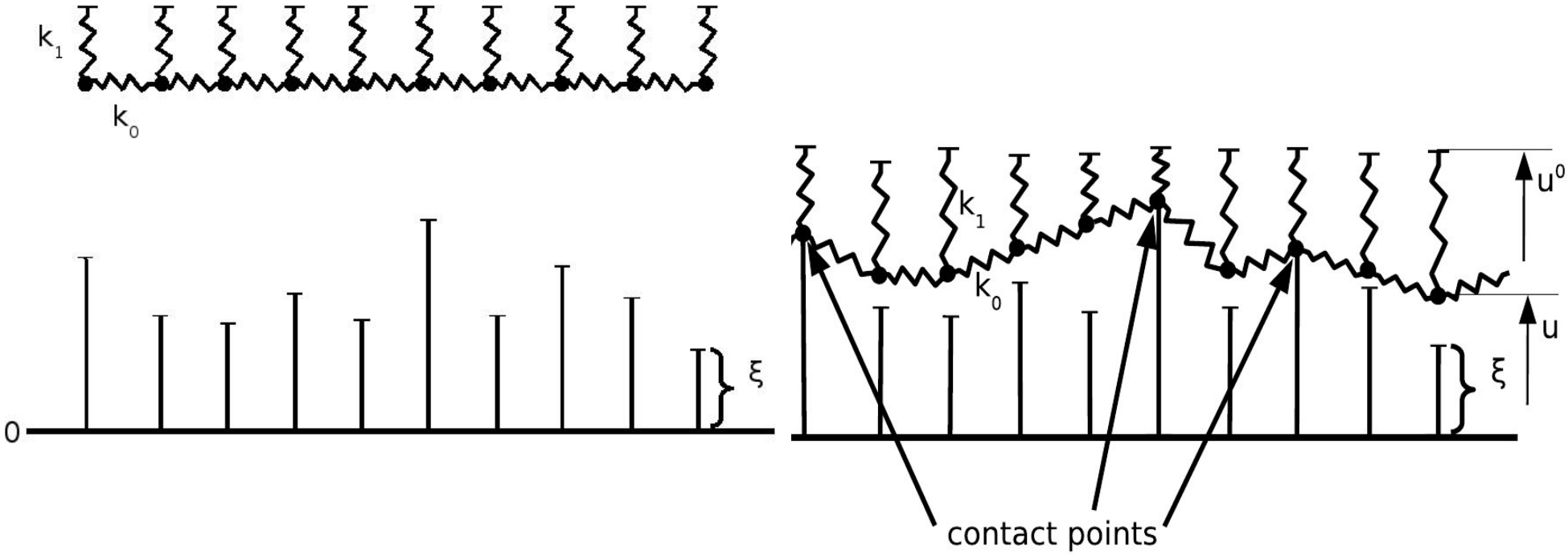

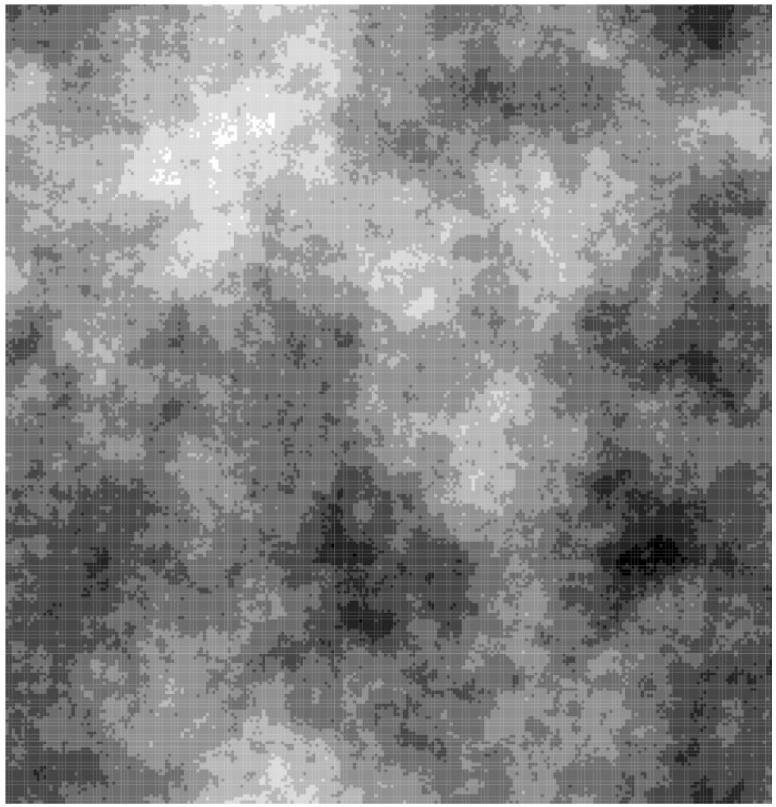

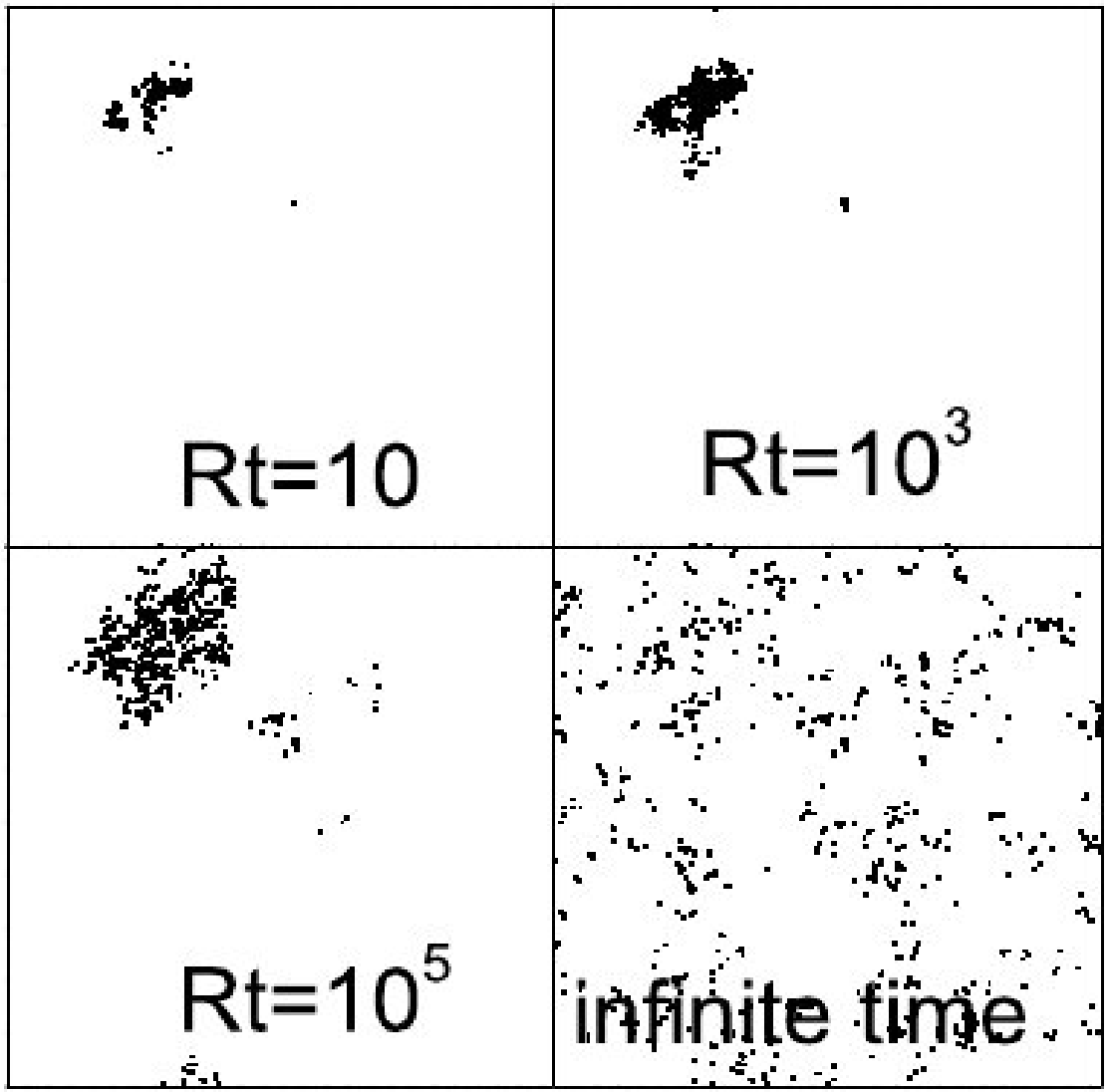
Rt=10
Rt=10^3
Rt=10^5
infinite time

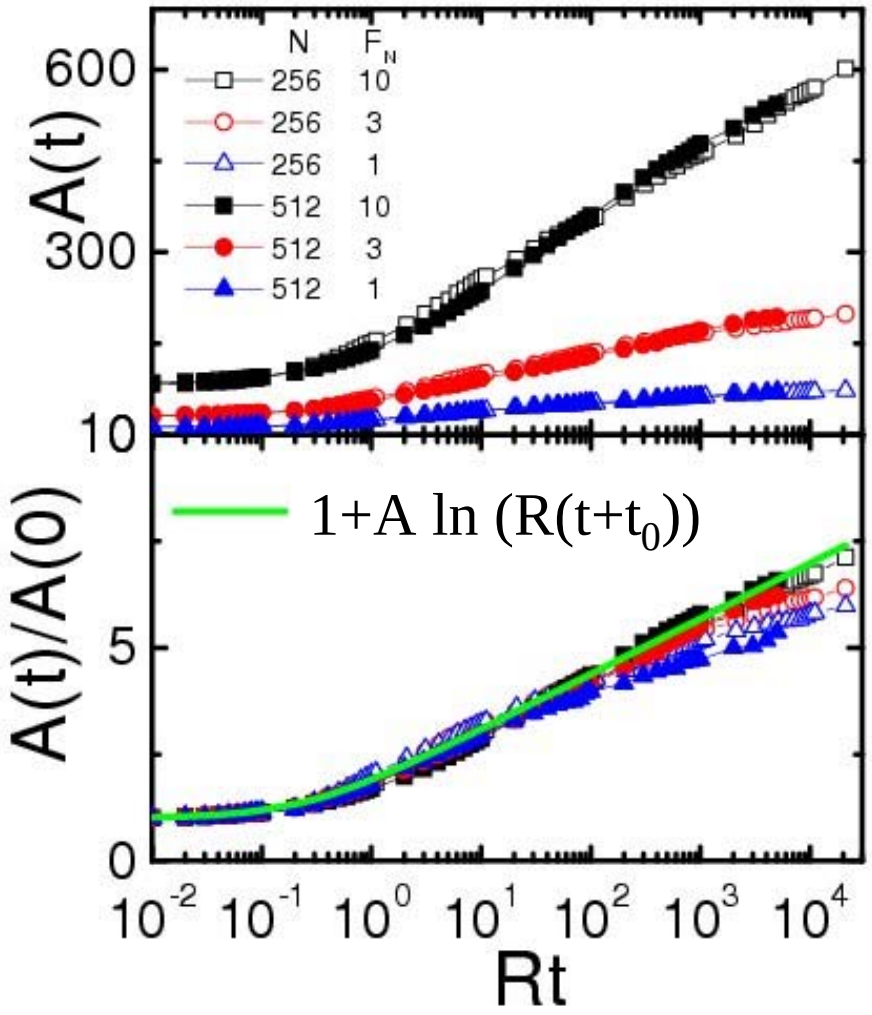
N
F_N
256 10
256 3
256 1
512 10
512 3
512 1
600
300
10
A(t)
1+A ln (R(t+t0))
A(t)/A(0)
5
0
10^{-2} 10^{-1} 10^{0} 10^{1} 10^{2} 10^{3} 10^{4}
Rt

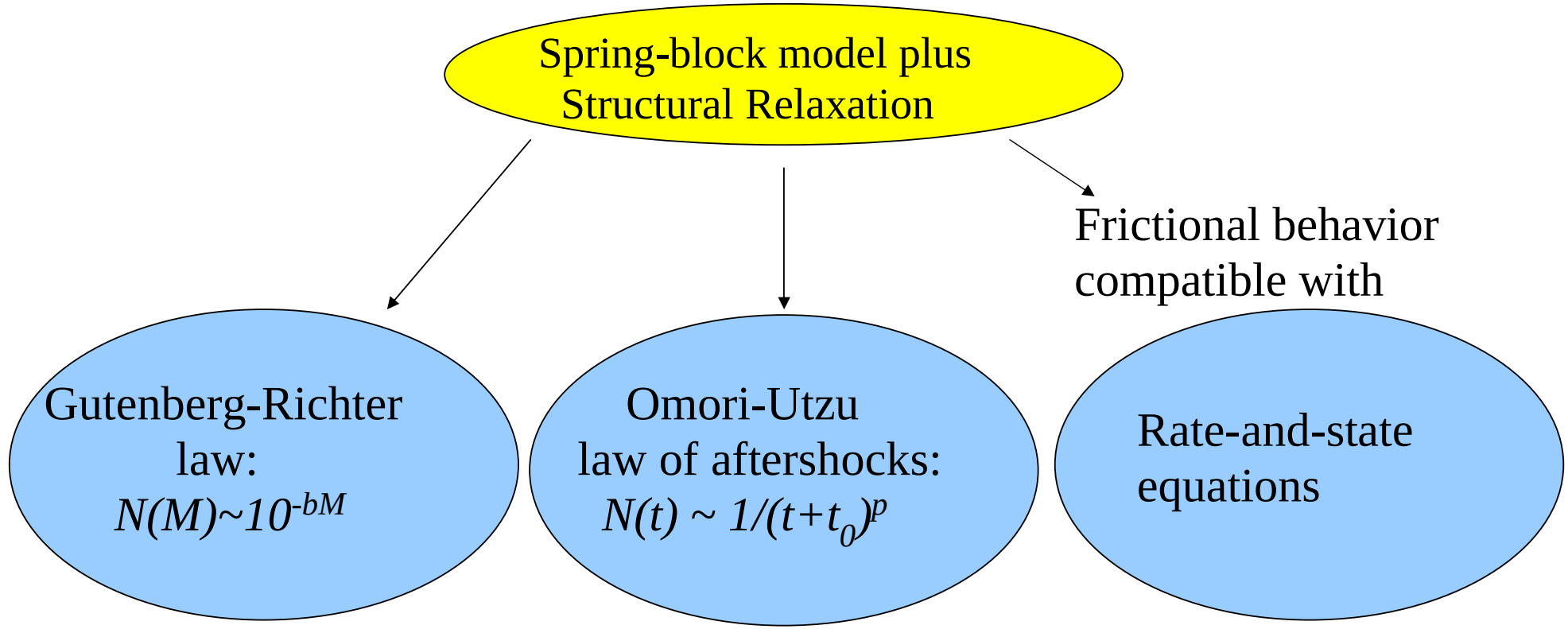

Robust b, around 1.1

'p' a bit large (~1-1.5)
It can be improved
(no long range elasticity
included up to now)

Very good agreement
with the phenomenology.
Model can be adapted
to show logarithmic
time increase of the
contact area


Thank you!
Hope to see you
in Bariloche
CONICET
CONSEJO NACIONAL
DE INVESTIGACIONES
CIENTÍFICAS Y TÉCNICAS
Instituto
Balseiro
Bariloche
CNEA

A mechanism for spatial and temporal earthquake clustering

E. A. Jagla and A. B. Kolton

Centro Atómico Bariloche, Comisión Nacional de Energía Atómica, 8400 Bariloche, Argentina

Abstract. The Gutenberg-Richter law states that the number of earthquakes as a function of magnitude decays as a power law. This trend is usually justified using spring-block models, where slips with the appropriate statistics of sizes have been numerically observed. However, prominent spatial and temporal clustering features of earthquakes, as those implied by the Omori law of aftershocks are not accounted for by this kind of models unless they are complemented with ad hoc assumptions, such as stress recovery laws after slip events, or the phenomenological rate-and-state equations to describe friction. We show that when an appropriate mechanism of structural relaxation is incorporated into a spring-block model, realistic earthquake patterns following in particular the Gutenberg-Richter and Omori laws are obtained. Moreover, velocity weakening and other features well known from laboratory friction experiments appear as a consequence of the relaxational mechanism as well, without making any a priori assumptions on the velocity dependence of the friction force in the model. In this way, our model shows that a single physical mechanism may be a unifying concept behind the Gutenberg-Richter and Omori laws, and the rate-and-state equations of rock friction.

1. Introduction

The distribution of earthquakes in nature follows non-trivial patterns, some of which are captured by two well known empirical laws, namely the Gutenberg-Richter law [*Gutenberg and Richter*, 1956], and the Omori (or Omori-Utsu) [*Omori*, 1894, *Utsu et al.*, 1995] law [*Scholz*, 2002; *Ben-Zion*, 2008]. The Gutenberg-Richter (GR) law states (in its cumulative form) that the number of earthquakes $N(M)$ with magnitude larger than M decreases as $N(M) \sim 10^{-bM}$. The exponent b has some regional variation, and it is typically found to be in the range 0.7-1.3 [e.g., *Frohlich and Davis*, 1993, *Utsu*, 1999, *Wiemer and Wyss*, 2002]. A power law distribution of earthquakes, as indicated by the GR law can be understood as originated in a state of (at least partial) self organized criticality of the system [*Bak et al.*, 1987; *Bak and Tang*, 1989; *Carlson et al.*, 1994], in which a power law distribution of events exists for a broad range of parameters. A number of statistical models generate a power law distribution of earthquakes. Among them, the pioneer is the model of Burridge and Knopoff [1967], that describes a collection of blocks (modeling small patches of a tectonic plate) connected elastically between nearest neighbors, and sliding on top of a rigid surface. The blocks are uniformly driven, simulating tectonic loading. The model assumes the knowledge of a prescribed friction law between blocks and substrate. A power law decay of number of earthquakes with magnitude (in a limited magnitude range) is obtained in the case in which the friction law displays velocity weakening (i.e., the friction force decreases with the relative velocity of the sliding elements [*Scholz*, 2002]). Other models, obtained as limiting cases of the BK model, or inspired on it, have been proposed that generate a GR power law distribution. Particular interest has been paid to the model by Olami, Feder, and Christensen [1992] (OFC), specially because of its simplicity, both in description and in numerical treatment. In this model, instead of the positions of the blocks, the variables are the values of the local friction forces for all spatial positions. These forces are evolved in time with the requirement that they must be lower than some maximum friction force, or threshold, otherwise a stress redistribution representing an earthquake occurs in the system. In most of these models, obtaining a realistic value of the decaying exponent b requires the adjustment of some parameter, i.e., a realistic value of b does not emerge as a robust feature.

The Omori law is the second quantitative law about distribution of earthquakes we consider. It refers to the temporal distribution of aftershocks, namely the temporal clustering of earthquakes following a large one, usually called the main shock. This law states that the number of aftershocks per unit of time decays as $\sim (t+c)^{-p}$ with the time t from the main shock. The exponent p is usually found to be close to 1, although other values and even other functional forms have been observed [*Ben-Zion*, 2008], and c is a time constant that depends on the low magnitude cutoff used, and that can vary between minutes and days. Aftershocks occur mainly close or within the spatial region where the rupture of the main shock took place. The origin of aftershocks has been controversial for very long time and many mechanisms have been considered in its explanation. Some of the physical processes invoked have included fluid flow following the main rupture [*Nur and Booker*, 1972], visco-elastic response [*Mikumo and Miyatake*, 1979], dynamic stress triggering [*Felzer and Brodsky*, 2006; *Gomberg et al.*, 1998], afterslip [*Perfettini and Avouac*, 2004; *Helmstetter and Shaw*, 2009], damage rheology [*Ben-Zion and Lyakhovsky*, 2006], and sub-critical crack growth [*Das and Scholz*, 1981; *Shaw*, 1993].

In a seminal work, Dieterich [1994] described aftershocks as a combination of static stress redistribution caused by the main shock, followed by failure under nearly constant stress conditions [*Scholz*, 1968; *Narteau et al.*, 2002]. The main idea of this line of thought is that after a main shock, parts of the fault close to the main rupture region are loaded to stresses that can be higher than its long-term strength, and thus this sector will fail in a finite time according to the laws of static fatigue processes. Assuming standard fatigue laws to hold, a prediction of a rate of aftershocks according to the Omori law has been obtained by different authors [*Dieterich*, 1994; *Marcellini*, 1997; *Helmstetter and Shaw*, 2006; *Zoller et al.*, 2005].

The failure by static fatigue is compatible with the description of the fault using the rate-and-state equations [*Dieterich*, 1979; *Ruina*, 1983] which in particular incorporate the process of velocity weakening.

0148-0227/09/$9.00

The description of the GR and the Omori laws in a unified framework has been, however, problematic. The statistical models that provide a reasonable justification for the GR law rarely show aftershocks, or other type of spatial or temporal correlation between events. It must be mentioned that the OFC model in its original form does display aftershocks [*Hergarten and Neugebauer*, 2002] but in our view these aftershocks are peculiar to details of the model, and do not account for actual aftershocks. In fact, aftershocks in the OFC model depend exclusively on tectonic loading, and stop immediately if this is halted. Although it is not possible experimentally to stop tectonic loading to see if aftershock cease, there is consensus [*Scholz*, 2002] that aftershocks should continue for same time under this hypothetical condition, indicating that they are dependent on some internal non stationary effect within the fault. In addition, we have found that aftershocks in the OFC model completely disappear if the threshold values, instead of being taken as uniform, are allowed to have spatial variations in a range as low as about 5 %. This points out to the fact that aftershocks are not a robust feature of the OFC model.

Ito and Matsuzaki [1990] were able to obtain aftershocks in a statistical model assuming fault strengthening or weakening after a block slips. An interesting attempt to obtain a statistical model that describes aftershocks in a realistic way has been made by Hainzl *et al.* [1999; 2000]. They used the OFC model incorporating partial stress recovery due to transient creep after the occurrence of events, following a prescribed function of time. In this way they are able to obtain aftershocks with many realistic properties. However, realistic values of the b decaying exponent of the GR law are obtained only after fine tuning of a parameter in the model.

The numerical description of a planar fault by a collection of pieces described by the rate-and-state equations was initiated by Dieterich [1995], and followed by Ziv and Rubin [*Ziv*, 2003; *Ziv and Rubin*, 2003]. They have shown that a collection of elements described by the rate-and-state equations with appropriate parameters can in principle describe both the GR law and the Omori law. Yet in this simulations the use of rate-and-state equations remains phenomenological, as the physics described by these equations has not been obtained up to now as a robust output of a statistical model with well defined microscopic laws. This is precisely what we do here.

We present a spring block type model that is inspired in the BK and the OFC models. The model is of Hamiltonian nature, namely, we define the energy of the model and evolve the variables according to a dynamics of the overdamped type. In particular, we do not need to introduce any ad hoc form of the friction law between blocks and substrate. We complement the model with an appropriate relaxational term as discussed below, intended to describe aging effects in the sliding bodies. With these ingredients we simultaneously obtain: 1) earthquake distributions and in particular aftershock sequences quantitatively comparable with real ones, 2) a velocity weakening friction law, and in general, agreement with the available experimental results in rock friction and 3) a power law decay for the number of earthquakes with magnitude compatible with the GR law, with an exponent b that compares well with actual values without fine tuning of parameters.

2. Model in the absence of relaxation

Our modeling is inspired in the BK model [*Burridge and Knopoff*, 1967], and also in the description of elastic manifolds driven on top of disordered media [*Fisher*, 1998]. A two-dimensional square arrangement of elements, or "blocks" (with periodic boundary conditions) is considered. A coordinate $u_{i,j}$, measuring the local displacement between block and substrate is assigned to one each element. Nearest neighbor blocks are connected by springs with spring constant k_0. The variables $u_{i,j}$ are driven externally through a spring of stiffness constant k_1 (see Fig. 1a). In addition, the cohesion between blocks and substrate is modeled by the use of a potential energy function $W_{i,j}(u)$ (specified below) that incorporates disorder, or "roughness", and that is chosen independently for each block label i, j. In this way, the energy E of the system reads

$$E = \sum_{i,j;i',j'} \frac{k_0}{2} (u_{i,j} - u_{i',j'})^2 + \sum_{i,j} \frac{k_1}{2} (U(t) - u_{i,j})^2 + \sum_{i,j} W_{i,j}(u_{i,j}) \tag{1}$$

where we note by i', j' a neighbor site to the i, j site, and $U(t)$ is the driving variable (usually we will choose $U(t) = Vt$, we will refer also to $U(t)$ and to $k_1(U(t) - u_{i,j})$ as the strain and local stress in the system, respectively).

One may think that in a more realistic description of sliding on a planar fault, the potential energy functions W should be considered to be correlated in some way. Several arguments point however against the existence of long-range correlations in W that might qualitatively alter the results obtained in the absence of correlations. A periodic array of elastically coupled blocks on top of a disordered substrate can display long-range periodic correlations and anisotropic response due to the discrete translation symmetry of the periodic system. This situation is however unstable under the presence of inhomogeneities in the elastic coupling constants [*Cule and Hwa*, 1996] and thus unlikely for the case of faults. Formally, this means that in our model, the sliding direction (i.e. along the "u" axis) does not correspond to any particular direction in the plane of the fault, but must be considered as a sort of independent direction. Also, from a purely practical point of view, the potential landscape is expected to irreversibly change after an earthquake, and correlations to be destroyed. We therefore take a disordered average pinning force correlator $\overline{W_{i,j}(u) W_{i',j'}(u')} \sim \delta_{i,j;i',j'} \Delta(u - u')$ with $\Delta(u)$ a short-ranged function. This makes the model based on Eq. (1) belong to the so-called random-manifold depinning universality class [*Chauve et. al.*, 2000; *Rosso et al.*, 2007] and thus to share universal critical exponents with other systems such as magnetic domain walls, as we will see below.

The time evolution of the variables $u_{i,j}$ are derived from the previous energy assuming an overdamped dissipative dynamics, i.e., neglecting inertia effects. Namely, we must solve the equations:

$$\frac{du_{i,j}}{dt} = -\lambda \frac{\delta E}{\delta u_{i,j}} \tag{2}$$

Once we specify the cohesive potentials between blocks and substrate $W_{i,j}(u)$, the previous equations allow to obtain the exact temporal evolution of $u_{i,j}$. We will work in the limit in which the relaxation time of Eq. (2) (proportional to λ^{-1}) is smaller than any other time scale in the system. We can consider formally that $\lambda \to \infty$. In this case the dynamics of the system has two qualitatively different parts. One of them consists in a quasistatic evolution of the variables, in which Eq. (2) is satisfied with a vanishing left hand side, i.e (from Eqs. (2 and 1)),

$$\sum_{i,j} k_0 (\nabla^2 u)_{i,j} + \sum_{i,j} k_1 (U(t) - u_{i,j}) = \sum_{i,j} \frac{dW_{i,j}}{du_{i,j}} \tag{3}$$

(∇^2 is the discrete Laplacian operator on the lattice, we will take the lattice constant as the unit of length). This equation states that the force onto each block exerted by all springs to which it is attached, has to be balanced by the

pinning force made by the substrate. The second mode of evolution occurs when, upon a slight increase of the external driving, Eq. (3) cannot be satisfied by a small rearrangement of the u's. In this case an abrupt rearrangement of the variables occurs, until Eq. (3) is satisfied again (see Fig. 1). These rearrangements correspond to the earthquakes (we call them also "events") in the system. In view of our choice $\lambda \to \infty$, we see that earthquakes, once triggered, occur instantaneously. The size of an earthquake is characterized by the sum of the individual increases $\Delta u_{i,j}$ of all the variables during the rearrangement process, namely

$$S = \sum_{i,j} \Delta u_{i,j}. \tag{4}$$

The quantity S is the analog in our model of the seismic moment. We can thus appropriately define the magnitude M of an earthquake as $M = 2/3 \log_{10} S$ to match the modified Richter scale up to an additive constant.

The model as stated has received a lot of attention to describe the collective jerky motion observed in many different systems such as Barkhausen noise in magnets [*Durin and Zapperi*, 2006], jumps in the creep motion of magnetic domain walls [*Lemerle et al.*, 1998, *Repain et al.* 2004], avalanches in the depinning of a contact-line of a fluid [*Moulinet et al.*, 2004], and dislocation or crack propagation [*Moretti et al.*, 2004, *Bonamy et al.*, 2008].

The model in its present form is known to generate events with a Gutenberg-Richter like decay. The value obtained for b is a robust universal result, independent of the details of the functions W (provided they are short-range correlated) and the values of spring constants. However, the numerical value turns out to be $b \simeq 0.4$ [*Rosso et al.*, 2009] well different from the value $b \simeq 1$ observed in actual seismicity. In this respect, Narayan and Fisher [1993] predicted (under some assumptions that were proved very recently using Functional Renormalization Group and numerical calculations [*Rosso et al.*, 2009]) the general scaling relation,

$$b = \frac{3}{2} - \frac{3}{d+\zeta}, \tag{5}$$

relating the analog of the GR exponent characterizing the scale invariant part of the distribution of avalanches, with the internal dimension d of the elastic manifold ($d = 2$ in our case of faults) and ζ the roughness exponent of the interface at the length scale where avalanches are produced. In other words, the size of an avalanche of linear size L scales as $S \sim L^{d+\zeta}$. For $d = 2$ the roughness exponent corresponding to the universality class of our model is found to be $\zeta \approx 0.75$ [*Rosso et al.*, 2003], yielding $b \approx 0.4$ in good agreement with recent numerical results [*Rosso et al.*, 2009].

2.1. Simplified treatment

In its present form the numerical simulation of the model is rather time consuming. In addition, in the next section we will incorporate additional degrees of freedom that further increase the simulation time. It is thus very convenient to have a limiting version of the model that adapts better to efficient numerical simulation without changing the basic properties of the original model. We will see that the derivation and the final version of the model shares many features with the model of Olami *et al.* [1992]. We describe now this version. We first note that the essence of Eq. (3) is to find values of the u's that correspond to mechanical equilibrium, i.e., in which to total force on each block vanishes. This means that for each block the substrate force $f = -dW/du$ has to balance the force from neighbors plus the force from driving. The friction force f has maxima as a function of u that are typically separated some distance δu that we associate with the slip distance of more phenomenological approaches [*Scholz*, 2002]. We will make a simplification by replacing the actual form of the local friction force by a set of "spikes" at the values of u corresponding to the maxima of f, and with the corresponding height (see Fig. 1b). In this way, given a fixed value of neighbors-plus-driving force, we will determine a value of u that has some error with respect to the correct value, the error being of order δu. Now we can see that if we maintain the spring constants k_1, and k_0 being much smaller than $F_0/\delta u$ (with F_0 being the typical height of the force maxima), then this error δu produces onto the neighbors a corresponding modification of the force and equilibrium positions that are of higher order in $k_{1,0}\delta u/F_0$, and can thus be ignored. This means that we can replace the true force from the substrate by a set of discrete values located at discrete positions, as indicated in Fig. 1b, if we accept inaccuracies of order δu in the values of $u_{i,j}$. These inaccuracies will in fact be acceptable for our analysis since reasonably large earthquakes will involve local re-arrangements of the variables that are much larger than δu, and then the previous definition of size S for the earthquakes still makes sense. We will set units such that $F_0 = 1$, and $\delta u = 1$. This means that the limit we are analyzing corresponds to $k_1 \ll 1$ and $k_0 \ll 1$. In the literature of elastic manifolds on random potentials, this limit where each block of the elastic object can be localized and individually pinned can be viewed as a strong zero-dimensional (i.e. point disorder) pinning. Interestingly, the modified model we propose here can be considered as the two dimensional generalization of the zero dimensional discrete model recently proposed by Le Doussal and Wiese [2009], with the difference that in our model the force spikes are randomly located (as it would be in a more realistic situation of strong pinning), instead of being located at all integers. In the next section we will show that our simplified model is in the same universality class of the original model derived from the energy functional of Equation 1. This imply that large scale properties, such as the avalanche or earthquake distributions, are not modified by our approximations.

This simplified form of the model admits a closed description in which we only focus attention on the local values of the friction force between block and substrate $f_{i,j}$, instead of on the values of $u_{i,j}$. In fact, given an initial set of values $f_{i,j}$, upon the application of the external driving the values of $f_{i,j}$ all increase at the same rate $k_1 V$. The system remains stable as long as all $f_{i,j}$ are lower than the corresponding maximum static friction force $F_{i,j}$ (the height of the spikes in Fig. 1b) that the block-substrate cohesion is able to sustain locally. When this maximum is overcome at some position, the block jumps to a new equilibrium position and the forces onto the neighbor sites are updated. Note that we do not need to generate the full sequence of force maxima and positions from the beginning. It is more efficient to generate them on the fly, as they are explored by the system.

In order to state the model to be simulated in the clearest terms, we rephrase the main dynamics as a sequence of rules:

1. Choose the threshold forces $F_{i,j}$ from a random Gaussian distribution with mean 1 and deviation σ_f.

2. Set all forces $f_{i,j}$ to zero at time $t = 0$ (dependence on initial conditions vanish after some transient period).

3. Increase all $f_{i,j}$ uniformly a small step $k_1 V \delta t$. Set $t = t + \delta t$. Repeat until $f_{i_0,j_0} > F_{i_0,j_0}$ at some site i_0, j_0.

4. Set S=0 and $(i_e, j_e) = (i_0, j_0)$ as the epicenter location.

5. Choose Δu from a random Gaussian distribution with mean 1 and deviation σ_x. Choose the new value of F_{i_0,j_0} from a random Gaussian distribution with mean 1 and deviation σ_f.

6. Decrease f_{i_0,j_0} to $f_{i_0,j_0} - (4k_0 + k_1)\Delta u$. Increase f on neighbor blocks in a quantity $k_0\Delta u$.

7. Set S=S+Δu.

8. Check if $f_{i_0,j_0} > F_{i_0,j_0}$ for some i_0, j_0. If yes, go to step 5. If not, declare that an event of size S at time t with epicenter (i_e, j_e) has occurred, and resume from step 3.

In this way, in step 3 a local instability of a given metastable state is fully developed by accumulation of stress, which can then trigger a global one (i.e. a cascade of instabilities or earthquake) which is fully developed from steps 4 to 8, until the system is in a more relaxed and new metastable state. Note that the choice of Gaussian distributions is just an approximation to more realistic distributions. In view of the independence of the results on the values of σ_f and σ_x (see results below) we do not expect any important dependence if other distributions with finite dispersion are chosen instead of the Gaussian, representing different short-ranged correlated random force fields. In this respect it is also worth pointing out here that the detailed form of the random force field, which can yield either a short-range (such as random-bond disorder in a magnet) or long-range correlated random potential (such as random-field disorder in a magnet), is irrelevant, since they belong to the same depinning universality class [*Chauve et al.*, 2000] (i.e. the two types of disorder yield the same dynamical critical fluctuations at vanishing velocities), at variance with the equilibrium problem where avalanches do in principle depend on the type of disorder (random-bond or random-field) [*Le Doussal et al.*, 2008].

Obvious additions to the previous algorithm can be implemented to calculate other quantities as needed. We want to emphasize the similarity of this approach to the one of Olami *et. al.* [1992]. It is important to make clear however, that although stated in a form that is typical of a system automaton, the previous sequence of rules solves the dynamical evolution Equations (1) and (2) in the quasistatic limit ($\lambda \to \infty$), with the only constraint that k_1, $k_0 \ll 1$. Moreover, we show below that our rules conduce to the well known critical properties of the model described by Equation 1.

The parameters of the model are the values of k_0 and k_1, and the dispersions σ_f and σ_x in the amplitudes and positions of the maximum local friction forces. Note in particular that the quantity $k_0/(4k_0 + k_1)$ corresponds to what in the OFC model is usually called α, varying between 0 and 0.25. We see that the derivation starting from a system with random local friction justifies immediately the use of a disordered distribution of maximum friction forces, or thresholds, $F_{i,j}$. This in turn produces remarkable differences of the results obtained compared to those obtained with the OFC model, as we will see below.

2.2. Results

We show now the results obtained by implementing the model presented above, in the limit corresponding to the set of rules stated at the end of the previous section. We will show results in our model for magnitudes larger than some cutoff M_0. We choose $M_0 = 0.7$ that corresponds to disregard events in which less than about 10 sites have participated, since these small events are strongly influenced from the numerical mesh we are using. In Fig. 2a we show the results for the distribution of events as a function of magnitude. We observe a power law with exponent $b \approx 0.4$, which is consistent with the expected results from the full implementation of a two dimensional elastic interface [*Rosso et al.*, 2009]. This shows that the simplified version of the model is in the same universality class than the original model of Equation 1. The value of the exponent is however well different from the $b \simeq 1$ observed for actual earthquakes. An exponential cut-off for large event size exists due to confinement, or in other words to the existence of a characteristic length-scale $L_1 \sim 1/\sqrt{k_1}$ associated with the drive which breaks the scale invariance for events with a linear size larger than L_1. This cut-off is controlled by the ratio k_1/k_0 of the driving spring to the spring between neighbors and occurs when the spatial extent of the events in the direction of the displacements is of order $L_1^\zeta \approx k_1^{-\zeta/2}$, with ζ the interface roughness exponent at low velocities. The crossover to the exponential behavior thus moves to larger magnitudes as k_1 is decreased [*Zapperi et al.*, 1998; *Lacombe et al.*, 2001; *Rosso et al.*, 2007; *Le Doussal et al.*, 2008] . In Fig. 2b we show a time-magnitude plot of all events occurring in a particular time interval. It is apparent that no obvious temporal correlations occur in this case. This is confirmed by an analysis of the time intervals between events of magnitude larger than some M_0, showing that the distribution of time intervals is essentially exponential, and independent of the precise value of the cut off M_0. This behavior was also recently found for static avalanches by Le Doussal *et al.* [2008]. We also mention that spatial correlations are neither observed in this case.

The present model generates a non-vanishing mean friction force that originates in the instabilities (earthquakes) that dissipate energy in the system. The mechanism is totally analog to that accounted for by the Tomlinson model, [*Braun*, 2004] which is one of the simplest examples where a finite friction force at a vanishing driving velocity is obtained due to slip weakening. In essence, although our dynamics is overdamped, and then dissipation vanishes for zero relative velocity between blocks an substrate, even a very small value of V produces abrupt rearrangements (earthquakes) that dissipate an amount of energy that does not vanish in the $V \to 0$ limit. It can be rigorously shown indeed, that due precisely to the presence of shocks or earthquakes, the average work done by the drive on a long distance is directly proportional to the critical depinning force [eg. *Rosso et al.*, 2007], which can only vanish for a very stiff interface $k_1 \to \infty$, or in the absence of disorder (i.e. the critical depinning force only depends on elasticity and disorder). In addition, the use of a rapid elastic relaxation ($\lambda \to \infty$) implies also that the actual value of external velocity V plays no role, and then the average friction force is constant and independent of V. In this sense, we can say that the frictional properties of the model in its present form are rather trivial. Note that in the case in which we use a finite value of λ, the friction force would get a contribution that is an increasing function of V. This would be the "direct effect" that is usually referred to in analysis based on rate-and-state equations [*Scholz*, 2002] which is not present in our case in which $\lambda \to \infty$. Since this part of the friction force comes from effective "viscous" forces that are not linked with instabilities but with the flow itself, our approximation cannot change the earthquake statistics in the limit of vanishing velocity.

3. Model in the presence of relaxation

In the present form, the model does not display earthquake clustering, and although it is explicitly constructed to have slip weakening, it does not display velocity weakening. Also, the decaying exponent in the GR law is not realistic. However, the inclusion of a simple additional ingredient changes this scenario drastically. This ingredient turns out to be what we have called *structural relaxation* [*Jagla*, 2007]. The primary physical justification of its inclusion is the following. It is known that in solid friction the static friction coefficient increases with the time the surfaces have been in contact [*Marone*, 1998b; *Persson*, 2000]. This means that the contact between surfaces strengthens as the contact time increases, and this has to be originated in some kind of time-dependent mechanism within the materials.

One simple form to introduce this effect in the kind of model we are studying, is to incorporate additional degrees of freedom that evolve through a slow relaxational dynamics controlled by the mechanical energy of the system. Consider a situation in which $V = 0$. In the model of the previous section, once Eq. (3) is satisfied (this occurs in a very short time scale) the energy of the system (Eq. (1)) stays constant. But if additional degrees of freedom exist, their evolution will make the energy of the system slowly decrease with time. This is a stabilization mechanism that in particular will strengthen effectively the cohesion between blocks and substrate as a function of time.

Let us see how this generic description can be implemented in concrete in our model. We will include for each position i, j an additional variable $u^0_{i,j}$ that corresponds to a global shift of the cohesive energy $W_{i,j}$. Concretely, the last term of Eq. (1) will be replaced according to

$$\sum_{i,j} W_{i,j}(u_{i,j}) \rightarrow \sum_{i,j} W_{i,j}(u_{i,j} - u^0_{i,j}) \tag{6}$$

Evolution of the u variables (Eq. (2)) stays formally the same as before. But now we give the substrate the possibility to react to the friction force by allowing a slow modification of the u^0 variables according to

$$\frac{du^0_{i,j}}{dt} = R\nabla^2 \frac{\delta E}{\delta u^0_{i,j}} \tag{7}$$

This dynamical evolution of the relative shift of the cohesive potential at different positions (see Fig. 1c) is a generic way to introduce the back effect of the sliding blocks onto the substrate. The coefficient R is a measure of the intensity or rate of relaxation, and can thus be related to experimental relaxation times. Since the variation of energy with respect to u^0 is simply the local friction force $f_{i,j}$, we see that Equation (7) generates a tendency for the forces $f_{i,j}$ to become uniform across the system, generating a stronger cohesion between the elastic surface and substrate. This relaxational effect competes with the driving, which forces the movement of the blocks onto the substrate at a fixed average velocity V and tends to de-correlate the values of $f_{i,j}$ at different spatial positions. Thus the relevant parameter that measures the competition between the two effects is the ratio R/V. We will show in the following that this relaxation mechanism produces the appearance of a robust sequence of aftershocks, and the occurrence of a velocity weakening friction law. Our structural relaxation mechanism is what in other contexts is called the aging of the material [e.g. *Cugliandolo*, 2002].

We want to point out that the use of the Laplacian in the right hand side of Eq. 7, instead of a purely local relaxation (in which the right hand side of Eq. 7 would be of the form $\sim -R\delta E/\delta u^0$) cannot be completely justified a priori. Let us say that this is the choice that gives the physical output we are searching for. Also, the use of the Laplacian implies (see results below) that if V is set to zero at some moment, the stresses in the system do not decay to zero with time (because the spatial mean value of u^0 does not evolve), a result that is consistent with what is observed for instance in rock friction stop-and-go experiments [*Marone*, 1998b], and that is not obtained if we use purely local relaxation.

In order to have a description in terms of the forces $f_{i,j}$ only, and a set of rules like those at the end of the previous section also in the presence of relaxation, we have to translate Eq. (7) to an evolution law for the forces $f_{i,j}$. This can be done easily in the approximation of the "spikes" already discussed. The result can be obtained by noticing that upon changes $\delta u_{i,j}$ of the variables, the forces change as

$$\delta f_{i,j} = (4k_0 + k_1)\delta u_{i,j} - k_0 \sum_{i',j'} \delta u_{i',j'} \tag{8}$$

where again i', j' are sites neighbors to the site i, j. Combined with Eq. (7) and taking into account that in the spike approximation changes in u^0 imply the same changes in u, we obtain

$$\frac{df_{i,j}}{dt} = k_1 R(\nabla^2 f)_{i,j} - k_0 R(\nabla^4 f)_{i,j} \tag{9}$$

In this way, the only modification we need to add to the list of rules of the previous section to take account of relaxation is:

3'- Modify all $f_{i,j}$ to the new values $f_{i,j} + k_1 V\delta t + (df_{i,j}/dt)\delta t$, where $df_{i,j}/dt$ is calculated from Eq. (9). Set $t = t + \delta t$. Repeat until $f_{i_0,j_0} > F_{i_0,j_0}$ at some site i_0, j_0.

3.1. Results and comparison with an actual earthquake sequence

Before showing the results we have obtained, it is necessary to mention that a quantitative detailed comparison between our results and those of actual seismic catalogs is not totally straightforward. The first reason is that actual earthquake catalogs do not correspond typically to a single planar fault. But beyond this obvious fact, although robust quantitative features like the GR, or Omori law can be tested with reasonable confidence, the analysis of other type of correlations between events, distributions of time interval among them, etc., have not found a unique way to be done on actual catalogs. Then although we are aware of few different attempts to characterize actual seismic sequences [*Corral*, 2004, 2005; *Baiesi and Paczusky*, 2004, 2005; *Zaliapin et al.*, 2008], at present we will not try to do a detailed comparison with these approaches, and focus only on some qualitative comparisons, and on the two robust quantitative features that are accepted by the community, namely the GR and Omori laws.

3.1.1. Some qualitative comparisons

In Fig. 3a we show a magnitude-time plot of events in a simulation of a system of 200×200 sites, in the presence of relaxation ($R/V = 5$). The changes with respect to the case without relaxation (Fig. 2b) are notorious. There is now an apparent temporal clustering of earthquakes following the largest ones. These largest events do not occur with any obvious periodicity, but seem to be more or less randomly located in time. For comparison, the equivalent plot for the earthquakes in the California area [*NCDEC and ANSS*, 2008] in which only events with $M > 2$ are considered, is presented as Fig. 3b. The visual similarity is striking.

The reason for the appearance of aftershocks in the presence of relaxation can be qualitatively understood in the following way. An event in the system is triggered each time the local friction force $f_{i,j}$ becomes larger than the local strength $F_{i,j}$. According to rule 3', $f_{i,j}$ can increase and trigger an event because of two reasons: the first one is the direct triggering produced by the term $k_1 V\delta t$. This is the triggering mechanism that exists in the model without relaxation. The second mechanism is triggering by the term $(df_{i,j}/dt)\delta t$, which exists only in the presence of structural relaxation. In fact, if $f_{i,j}$ fluctuates spatially, this term may produce the increase of $f_{i,j}$ at some points, eventually overpassing the local strength and triggering an event. These are aftershocks. Note that if relaxation has acted for a long time, $f_{i,j}$ will be rather uniform spatially, and aftershocks will be much less abundant. This internal aging mechanism justifies the observation that aftershock rate decreases progressively after the main shock in the model.

Figure 4 shows plots of cumulated number of events and seismic moment corresponding to the sequences presented in Fig. 3, and Fig. 5 is a detail after the events indicated by vertical arrows in Fig. 4. In Fig. 5 the cumulative number

of events after the large event is compared with a cumulative Omori law, with $p = 1$. The evolution of the accumulated seismic moment is also qualitatively similar in both cases, with the main shock accounting for most of the released seismic moment of the whole sequence.

3.1.2. Gutenberg-Richter behavior

The inclusion of relaxation produces a change in the decaying exponent b of the GR law. In Fig. 6 we see that in the presence of relaxation, the b value is substantially larger than the one corresponding to no relaxation. More than that, there seems to be a convergence to a well defined exponent b^* once a minimum value of relaxation has been over passed (about $R/V \sim 1$). Remarkably, we obtain that b^* is approximately 1.1, quite independently of the parameters k_1, k_0, σ_f, σ_x, i.e., in the range of experimentally observed values. The GR law in the presence of relaxation continues to have a cut off for large event sizes that is mainly dependent on the ratio k_1/k_0. The smaller this value, the larger is the cut-off, as can be seen in Fig. 6a.

The fact that the b exponent converges to the b^* value for large relaxation, independently of other model parameters seems to indicate that relaxation is a relevant variable (in the language of renormalization group) and takes the system out of its original universality class with $b \simeq 0.4$, characterizing the avalanches of two dimensional interfaces with short-range elasticity in an uncorrelated quenched random potential, to a new one with $b = b^*$. The fact that b^* is compatible with actual values from real seismicity is an indication that we are probably capturing essential (large-scale) features of the seismic process with the inclusion of the relaxation mechanism.

3.1.3. Omori law

The apparent existence of aftershocks observed in the numerical results in Fig. 3 can be put on more quantitative bases by fitting it to the Omori law. In Fig. 7 we plot an histogram with the number of events after main shocks as a function of time. In the simulations, we average over 450 large events with $M > 3$ in a single simulation of size 200×200, and count only events larger than the threshold magnitude $M_0 = 1.5$. For comparison the same plot for earthquakes in the California area is also shown (lower cut-off magnitude $M_0 = 2$). The continuous lines correspond to an Omori laws of the form $N(t) = A/(t + c)^p + N_0$, where t is the time since the main shock and N_0 is the value of background seismicity. We find for our results that typically the best fitting is obtained with values of p around 1.5, which corresponds approximately to the maximum values that are experimentally observed [*Utsu et al.*, 1995].

In the model, the main factor that controls the production of aftershocks is the value of R/V. For $R/V \lesssim 1$ almost no aftershocks are observed (note that this value was also mentioned as the value for which the GR law has acquired its asymptotic form, with a decaying exponent b^*). On the other hand, going to very large values of R/V produces an over-abundance of aftershocks, since in this case the time interval between main shocks (depending inversely on the small V value) becomes extremely large. There must be noticed also that the apparent rate of aftershock production in the model and also in actual seismicity depends on two additional variables. One is the spatial extent of the region considered, in our case, on system size. This is clear because in a larger system with same parameters the aftershocks will occur on top of a background seismicity rate that is proportionally larger. The second variable is the lower magnitude cutoff M_0 used in counting aftershocks. Typically, a larger value of M_0 leads to a greater relative abundance of aftershocks, compared with background seismicity, both in our model and for actual seismic data. The parameters in Fig. 7 were chosen to produce approximately the same abundance of aftershocks in our running and in the California database.

The spatial location of aftershocks epicenters in the model is strongly correlated with the slip surface of the associated main shock. In Fig. 8 we show the regions that slip before, at, an after a particular large event in the simulations, together with the epicenters of all events contributing to slip. Aftershocks in our model occur typically at the surface of previous slip, and only few of them in the adjacent region. However, aftershocks can have epicenters in the slip region of other previous aftershocks, and in this way the slip region can increase along the sequence, as it is particularly observed in Fig. 8(c-d). Actual aftershocks are known to occur both at, and near the main slip surface, probably with a larger fraction of events outside the main slip surface than in our model [*Scholz*, 2002]. We think the difference is due to the fact that we have not considered realistic (long range) elastic interactions in the model, that are responsible for remote stress increase after the main slip. Instead, our model only has nearest neighbors interactions and in this way aftershocks are not expected to occur away of the previous slip surface.

3.1.4. Stress drop

An experimental plot of seismic moment as a function of linear dimensions of the broken region, is known to follow a linear regression in logarithmic scale [*Scholz*, 2002]. The slope is found to be close to 3, and this is interpreted as an indication of a constant stress drop, independent of the earthquake magnitude. The plot made for our results (an example is contained in Fig. 9) shows also the same linear regression in logarithmic scale. A power law fitting gives values of the exponent between 2.5 and 3, which is just a bit smaller than actual values. It is interesting to interpret these results from a geometrical point of view. If the successive metastable states of the elastic surface have a self-affine structure, as it does in the absence of structural relaxation [*Rosso et al.* 2007], the seismic moment or volume S of an earthquake can be written in terms of the linear size of rupture L as,

$$S \sim L^{2+\zeta} \tag{10}$$

with ζ the corresponding roughness exponent. In this context the constant stress drop interpretation is related with the self-affinity, or to the absence of a characteristic length-scale (besides the cut-off controlled by k_1). Interestingly, in the absence of structural relaxation we have $\zeta \approx 0.75$, [*Rosso et al.*, 2003] and thus $S = L^{2.75}$ which is very close to the result of Fig. 9. This indicates that although structural relaxation is essential to obtain a more realistic GR law and to produce aftershocks described by the Omori law, it does not change appreciable the scaling of the seismic moment with the linear rupture size, seemingly suggesting that the effective roughness exponent remains unchanged under the relaxational mechanism. One could also ask whether the Eq. 5 relating ζ with the GR exponent b, conjectured and proved in the absence of structural relaxation, is still valid in the presence of it. At this point these issues remain unclear. The additional problem being here that in the presence of structural relaxation there exists a characteristic length (i.e., the length scale of the relaxed region between jumps) controlled by the ratio R/V unlike the case without relaxation. A detailed geometrical analysis of the sliding surface, particularly regarding the possible crossovers as a function of length-scale is thus needed and remains as a future prospect.

4. Frictional properties

In addition to the finding of earthquake clustering and a realistic GR behavior, a fundamental part of our work is to show that structural relaxation produces non trivial frictional properties in the system. First of all we recall that in the model without relaxation the average stress σ is independent of the strain rate, since the internal time scale of the

model is very rapid ($\lambda \to \infty$). The inclusion of relaxation introduces a new time scale (set by the parameter R in Eq. (7)) and now the average stress in the system depends on the ratio R/V. When R/V is small, the effect of relaxation is negligible, and the stress is similar to that in the absence of relaxation. However, if R/V is high enough, relaxation will act by effectively enhancing the cohesion between the set of sliding blocks and the substrate producing a larger average stress in the system. We then expect that the larger is R/V the larger will be the average stress. In other words, the model will display velocity weakening. In Fig. 10a we show a plot of the stress in the system as a function of strain rate where this weakening is clearly observed. For large strain rates the stress converges to the value corresponding to no relaxation, whereas the behavior for very small strain shows a saturation at a larger value. The transition between these two values is logarithmic and spans about a factor of 100 of strain rate. Note that the values reported above as necessary to observe aftershocks ($R/V \gtrsim 1$) correspond to the limit of small velocity in this plot, where the average stress has already reached its asymptotic value. This is not contradictory with experiments [*Baumberger and Caroli*, 2006; *Marone*, 1998a, 1998b], where velocity weakening is typically observed in the range of V between approximately 10^{-2} to 10^{2} $\mu m/s$, whereas tectonic loading is typically in the range of 10^{-4}-10^{-5} $\mu m/s$. A closer examination of the instantaneous stress-strain relation in the model (in Fig. 10a) reveals that the lower the strain rate, the more pronounced the fluctuations in the instantaneous stress.

Additional information on the frictional behavior is obtained by studying the system response to abrupt changes of the strain rate. We show in Fig. 10b in particular, the stress on a system in which driving is stopped during some time interval (the hold time) and then is re-initiated. First of all, a logarithmic decrease of stress during the hold time is observed. This occurs because the system continues to relax during the hold time and some instability events continue to occur for some time. This is related to our previous statement that aftershocks also occur if driving is stopped after a main shock. Despite the stress reduction during the hold time, a stress peak occurs after re-initiation of sliding. The height of this peak increases logarithmically with the hold time. This peak is a consequence of the more stable configuration that the system reached due to relaxation during the hold time. The phenomenon is similar to the one observed in glass forming materials [*Ho Huu and Vu-Khanh*, 2003; *Govaert et al.,* 2001; *Johnson et al.,* 2002], where it has been explained using the same ideas [*Jagla*, 2007]. These results are in remarkable agreement with those obtained in laboratory measurements [*Marone*, 1998a, 1998b]. In particular, the experimental finding of a logarithmic dependence of the dynamic friction coefficient on sliding velocity, and of the static friction coefficient on hold time are the base on which the phenomenological rate-and-state equations have been constructed. Here, these logarithmic dependences appear as a consequence of the "microscopic" (i.e. at the level of description of individual blocks) mechanism of structural relaxation. Also, the typical experimental values for the change of static (or dynamic) friction coefficient per order of magnitude of hold time (or relative velocity), is systematically found to be in the range of a few percents per decade [*Baumberger and Caroli,* 2006]. Remarkably, this is also the variation range that is observed in our results in Fig. 10.

5. Summary and Conclusions

In the present paper we have presented a modeling that combines a spring-block type system in the spirit of the BK and OFC models, ideas from the universal dynamics of elastic manifolds driven on disordered potentials, and a rather generic implementation of aging effects within the sliding materials. The motivation for this approach was to introduce, in a statistical model of solid friction and seismicity, a single mechanism that generates (and not merely assumes) non trivial frictional effects and at the same time produce realistic temporal and spatial clustering of earthquakes. Our model allows to obtain a temporal sequence of events that globally follow the GR law with a $b \simeq 1.1$ exponent, and at the same time non-trivial spatial and temporal correlations which are compatible, in particular, with the Omori law. In addition we have shown that frictional properties of the model compare very well with laboratory results. The consideration of the relaxation mechanism has thus allowed us to obtain a unified and comprehensive physical picture of these phenomena and also to make a definite connection with the physics of different disordered elastic systems which are common in condensed matter.

Beyond the interest the model may have based on the phenomenology it is able to reproduce, the unifying concepts we propose can be further tested by predicting with our model other interesting seismic properties. In particular it would be interesting to study to what extent the appearance of large events in the model can be anticipated assuming only partial knowledge about the state of the system. Whether the generic structural relaxational mechanism we describe here plays also a central role in other driven systems displaying jerky motion is another interesting open issue.

Acknowledgments.
This research was financially supported by Consejo Nacional de Investigaciones Científicas y Técnicas (CONICET), Argentina. Partial support from grant PICT 32859/2005 (ANPCyT, Argentina) is also acknowledged.

References

Baiesi, M., and M. Paczusky (2004), Scale-free networks of earthquakes and aftershocks, *Phys. Rev. E, 69*, 0661061-0661068.

Baiesi, M., and M. Paczusky (2005), Complex networks of earthquakes and aftershocks, *Nonlinear Processes Geophys., 12*, 1-11.

Bak, P., and C. Tang (1989), Earthquakes as a Self-Organized Critical Phenomenon, *J Geophys. Res., 94*, 15635-15637.

Bak, P., C. Tang, and K. Wiesenfeld (1987), Self-organized criticality: An explanation of the 1/f noise, *Phys. Rev. Lett., 59*, 381-384.

Baumberger, T., and C. Caroli (2006), Solid friction from stick-slip down to pinning and aging, *Adv. Phys., 55*, 279-348.

Ben-Zion, Y. (2008), Collective behavior of earthquakes and faults: Continuum-discrete transitions, progressive evolutionary changes, and different dynamic regimes, *Rev. Geophys., 46*, RG4006, doi:10.1029/2008RG000260.

Ben-Zion, Y., and V. Lyakhovsky (2006), Analysis of aftershocks in a Lithospheric model with seismogenic zone governed by damage rheology, *Geophys. J. Int., 165*, 197-210, doi:10.1111/j.1365-246X.2006.02878.x.

Bonamy, D., S. Santucci, and L. Ponson (2008), Crackling dynamics in material failure as the signature of a self-organized dynamic phase transition, *Phys. Rev. Lett., 101*, 045501.

Braun, O. M. (2004) *The Frenkel-Kontorova model: concepts, methods and applications*, Springer, 2004.

Burridge, R., and L. Knopoff (1967), Model and theoretical seismicity, *Bull. Seismol. Soc. Am., 57*, 341-362.

Carlson, J. M., J. S. Langer, and B-E. Shaw (1994), Dynamics of earthquake faults, *Rev. Mod. Phys., 66*, 657-670.

Chauve P., Giamarchi T., and Le Doussal P. (2000), Creep and depinning in disordered media, *Phys. Rev. B, 62* 6241-6267.

Corral, A. (2004), Long-term clustering, scaling, and universality in the temporal occurrence of earthquakes, *Phys. Rev. Lett., 92*, 108501-4.

Corral, A. (2005), Renormalization-group transformation and correlations of seismicity, *Phys. Rev. Lett., 95*, 028501-4.

Cugliandolo L. F. (2002), *Dynamics of glassy systems in Slow relaxation and nonequilibrium dynamics in condensed matter*, Editors: J. L. Barrat et al., Springer-Verlag.

Cule D. and Hwa T. (1996), Tribology of Sliding Elastic Media, *Phys. Rev. Lett., 77*, 278 - 281

Das, S., and C. H. Scholz (1981), Theory of time-dependent rupture in the Earth, *J. Geophys. Res., 86*, 6039-6051.

Dieterich, J. H. (1979), Modeling of rock friction .1. Experimental Results and Constitutive Equations, *J. Geophys. Res., 84*, 2161-2168.

Dieterich, J. H. (1994), A constitutive law for rate of earthquake production and its application to earthquake clustering, *J. Geophys. Res., 99*, 2601-2618.

Dieterich, J. H. (1995), Earthquake simulations with time-dependent nucleation and long-range interactions,*Nonlinear Processes Geophys., 2*, 109-120.

Durin G. and S. Zapperi (2006), The Science of Hysteresis, vol. II, G. Bertotti and I. Mayergoyz eds, Elsevier, Amsterdam, 181-267.

Felzer, K. R., and E. E. Brodsky (2006), Decay of aftershock density with distance indicates triggering by dynamic stress, *Nature, 441*, 735-738.

Fisher, D. S. (1998), Collective transport in random media: from superconductors to earthquakes, *Physics Reports, 301*, 113-150.

Frohlich, C., and S. D. Davis (1993), Teleseismin *b* values; or, much ado about 1.0.*J. Geophys. Res., 98*, 631-644.

Gomberg, J., N. M. Beeler, M. L. Blanpied, and P. Bodin (1998), Earthquake triggering by transient and static deformation, *J. Geophys. Res., 103*, 23,411-24,426.

Govaert, L. E., H. G. H. van Melick, and H. E. H. Meijer (2001), Temporary toughening of polystyrene through mechanical preconditioning, *Polymer, 42*, 1271-1274.

Gutenberg, B., and C. F. Richter (1956), Magnitude and energy of earthquakes, *Ann. Geophys.* (C.N.R.S) 9:1.

Hainzl, S., G. Zoller, and J. Kurths (1999), Similar power laws for foreshocks and aftershocks sequences in a spring block model for earthquakes, *J. Geophys. Res., 104*, 7243-7253.

Hainzl, S., G. Zoller, and J. Kurths (2000), Self-organization of spatio-temporal earthquake clusters, *Nonlin. Proc. Geophys., 7*, 21-29.

Helmstetter, A., and B. E. Shaw (2006), Relation between stress heterogeneity and aftershock rate in the rate-and-state model, *J. Geophys. Res., 111*, B07304.

Helmstetter, A., and B. E. Shaw (2009), Afterslip and aftershocks in the rate-and-state friction law, *J. Geophys. Res., 114*, B01308, doi:10.1029/2007JB005077.

Hergarten, S., and H. J. Neugebauer (2002), Foreshocks and Aftershocks in the Olami-Feder-Christensen Model, *Phys. Rev. Lett., 88*, 2385011-4.

Ho Huu, C, and T. Vu-Khanh (2003), Effects of physical aging on yielding kinetics of polycarbonate, *Theoretical and Applied Fracture Mechanics, 40*, 75-83

Ito, K., and M. Matsuzaki (1990), Earthquakes as Self-Organized Critical Phenomena, *J. Geophys. Res., 95*(B5), 6853-6860.

Jagla, E. A., (2007), Strain localization driven by structural relaxation in sheared amorphous solids, *Phys. Rev. E, 76*, 0461191-7.

Johnson, W. L., Jun Lu and Marios D. Demetriou (2002), Deformation and flow in bulk metallic glasses and deeply undercooled glass forming liquidsa self consistent dynamic free volume model, *Intermetallics, 10*, 1039-1046.

Lacombe, F., S. Zapperi, and H. J. Hermann (2001), Force fluctuation in a driven elastic chain, *Phys. Rev. B, 63*, 1041041-7.

Le Doussal P., and Wiese K.J. (2009), Driven particle in a random landscape: disorder correlator, avalanche distribution and extreme value statistics of records, *Phys. Rev. E, 79*, 051105-051145.

Le Doussal, P., A. Middleton, and K. J. Wiese (2008), Statistics of static avalanches in a random pinning landscape, *arXiv*:0803.1142v1.

Lemerle, S., J. Ferré, C. Chappert, V. Mathet, T. Giamarchi, and P. Le Doussal (1998), Domain wall creep in an Ising ultrathin magnetic film, *Phys. Rev. Lett., 80*, 849.

Marcellini, A. (1997), Physical model of aftershock temporal behavior, *Tectonophysics, 277*, 137-146.

Marone, C. (1998a), The effect of loading rate on static friction and the rate of fault healing during the earthquake cycle, *Nature, 391*, 69-72.

Marone, C. (1998b), Laboratory-Derived Friction Laws and their Application to Seismic Faulting, *Annu. Rev. Earth Planet. Sci., 26*, 643-696.

Mikumo, T., and T. Miyatake (1979), Earthquake sequences on a frictional fault model with non-uniform strengths and relaxation times, *Geophys. J. R. Astron. Soc., 59*, 497-522.

Moretti, P., M. C. Miguel, M. Zaiser, and S. Zapperi (2004), Depinning transition of dislocation assemblies: Pileups and low-angle grain boundaries, *Phys. Rev. B, 69*, 214103.

Moulinet, S., A. Rosso, W. Krauth, and E. Rolley (2004), Width distribution of contact lines on a disordered substrate, *Phys. Rev. E, 69*, 035103.

Narayan, O., and D.S. Fisher (1993), Threshold critical dynamics of driven interfaces in random media, *Phys. Rev. B, 48*, 7030-7042.

Narteau, C., P. Shebalin, and M. Holschneider (2002), Temporal limits of the power law aftershock decay rate, *J. Geophys. Res., 107*,(B12), 2359, doi:10.1029/2002JB001868.

Northern California Earthquake Data Center (NCEDC) and Advanced National Seismic System (ANSS) (2008), Earthquakes in the region between 115 and 119 W, and between 32 and 35 N, of $M > 2$ between January 1st (1980), and May 20th (2008), *ANSS/CNSS Worldwide Earthquake Catalog*, http://quake.geo.berkeley.edu/anss.

Nur, A., and J. R. Booker (1972), Aftershocks caused by pore fluid flow?, *Science, 175*, 885-887.

Olami, Z., H. J. S. Feder, and K. Christensen (1992), Self-organized criticality in a continuous, nonconservative cellular automaton modeling earthquakes, *Phys. Rev. Lett., 68*, 1244-1247.

Omori, F. (1894), On the aftershocks of earthquakes, J. Coll. Sci. Imp. Univ. Tokio, 7, 111-200.

Perfettini, H., and J. -P. Avouac (2004), Postseismic relaxation driven by brittle creep: A possible mechanism to reconcile geodetic measurements and the decay rate of aftershocks, application to the Chi-Chi earthquake, Taiwan, *J. Geophys. Res., 109*, B02304, doi:10.1029/2003JB002488.

Persson, B. N. J. (2000), *Sliding Friction, Physical Principles and Applications*, Springer, Berlin.

Repain, V., M. Bauer, J.-P. Jamet, J. Ferré, A. Mougin, C. Chappert, and H. Bernas (2004), Creep motion of a magnetic wall: Avalanche size divergence, *EPL (Europhysics Letters), 68*, 460-466.

Rosso, A., A.K. Hartmann and W. Krauth (2003), *Depinning of elastic manifolds*, *Phys. Rev. E, 67* 021602.

Rosso, A., P. Le Doussal, and K. J. Wiese (2007), Numerical calculation of the functional renormalization group fixed-point functions at the depinning transition, *Phys. Rev. B, 75*, 220201(R).

Rosso, A., P. Le Doussal, and K. J. Wiese (2009), Avalanche-size distribution at the depinning transition: A numerical test of the theory, *arXiv:0904.1123v1*.

Ruina, A. (1983), Slip Instability and State Variable Friction Laws, *J. Geophys. Res., 88*, 10359-10370.

Shaw, B. E.(1993), Generalized Omori law for aftershocks and foreshocks from a simple dynamics, *J. Geophys. Res. Lett., 20*, 907-910.

Scholz, C. H. (1968), Microfractures, aftershocks, and seismicity, *Seismol. Soc. Am. Bull., 58*, 1117-1130.

Scholz, C. H. (2002), *The Mechanics of Earthquakes and Faulting*, Cambridge University Press, Cambridge, England.

Utsu, Y. (1999), Representation and analysis of the earthquake size distribution: A Historical review and some new approaches, *Pure Appl. Geophys., 155*, 509-535.

Utsu, T., Y Ogata, and R. S. Matsu'ura (1995), The centenary of the Omori Formula for a decay law of aftershock activity,*J. Phys. Earth, 43*, 1-33.

Wiemer, S., and M. Wyss (2002), Mapping spatial variability of the frequency-magnitude distribution of earthquakes, *Adv. Geophys., 45*, 259-302.

Zaliapin, I., A. Gabrielov, V. Keilis-Borok, and H. Wong (2008), Clustering Analysis of Seismicity and Aftershock Identification, *Phys. Rev. Lett. 101*0185011-0185014.

Zapperi, S., P. Cizeau, G. Durin, and H. E. Stanley (1998), Dynamics of a ferromagnetic domain wall: Avalanches, depinning transition, and the Barkhausen effect, *Phys. Rev. B, 58*, 6353-6366.

Ziv, A. (2003), Foreshocks, aftershocks, and remote triggering in quasi-static fault models, *J. Geophys. Res., 108*(B10), 2498, doi:10.1029/2002JB002318.

Ziv, A., and A. M. Rubin (2003), Implications of rate-and-state friction for properties of aftershock sequence: Quasi-static inherently discrete simulations, *J. Geophys. Res., 108*(B1), 2051, doi:10.1029/2001JB001219.

Zoller, G., S. Hainzl, M. Holschneider, and Y. Ben-Zion (2005), Aftershocks resulting from creeping sections in a heterogeneous fault, *Geoph. Res. Lett., 32*, L03308, doi:10.1029/2004GL021871.

E. A. Jagla, Centro Atómico Bariloche, Comisión Nacional de Energía Atómica, 8400 Bariloche, Argentina (jagla@cab.cnea.gov.ar)

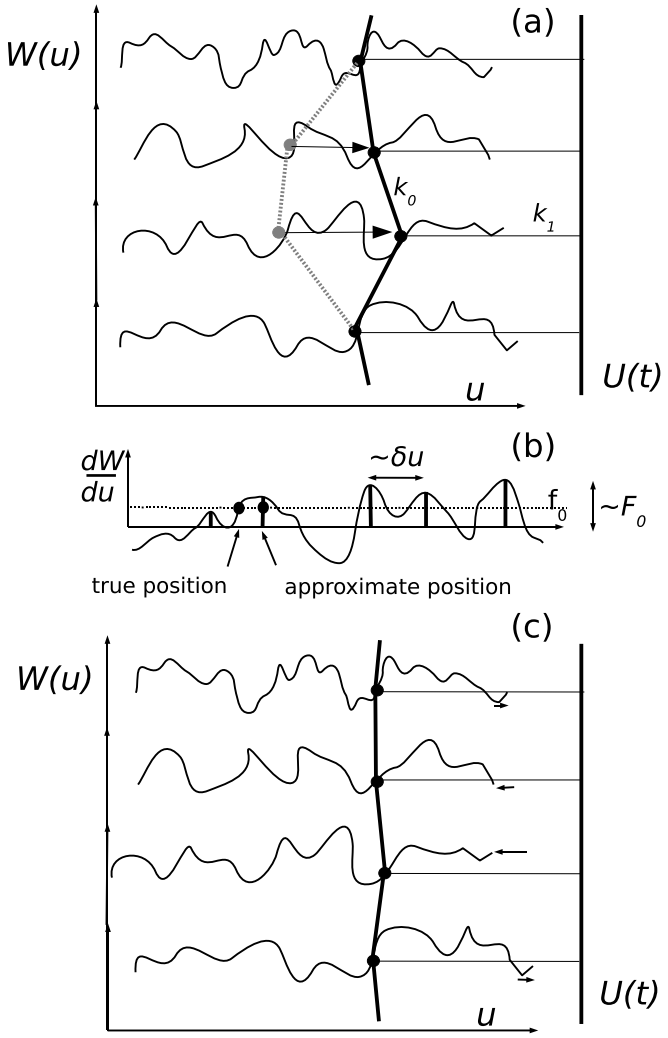

Figure 1. (a) One dimensional sketch of the model. The form of local (random) cohesive energies are shown for four different positions on the substrate, on which blocks (represented by the circles) slide. Driving through springs with stiffness constant k_1 pulls uniformly onto the blocks from the right. A locally stable configuration is shown with dotted lines, and the configuration after an event (an earthquake) induced by a small increase of the driving is shown in black. (b) Simplified form of the substrate interaction, in which the full force corresponding to a potential energy W is replaced by a set of spikes (of typical height F_0, and separated a typical distance δu) occurring at the places where the force is maximum. A given external force f_0 (horizontal dotted line) produces an equilibrium value of u using the simplified force, that differs by an amount of order δu from that using the correct force. (c) Effect of the relaxation mechanism. The global position of the cohesive potential at different points slowly accommodated (the individual shifts are indicated by the small arrows on the right) with respect to the configuration in (a) in order to reduce the total energy of the system, generating a more stable configuration.

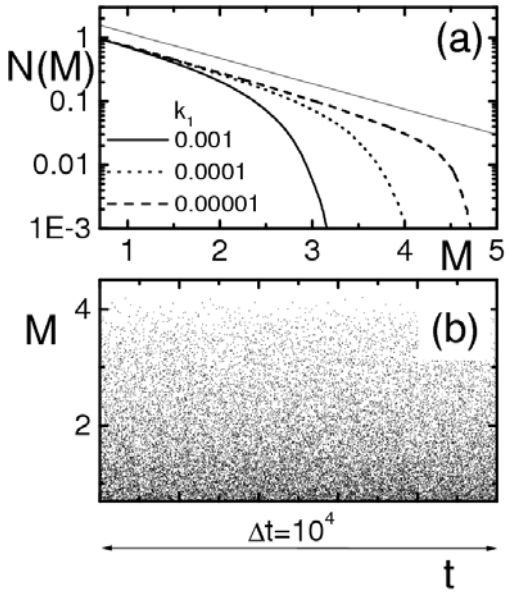

Figure 2. Results without relaxation. (a) Magnitude histogram for systems of 200×200 sites, with the values of k_1 as indicated, and with $k_0 = 0.1$, $\sigma_f = 0.8$, $\sigma_x = 0.8$. The thin straight line has a slope $b = 0.4$. (b) Magnitude-time plot corresponding to the case $k_1 = 10^{-4}$ in (a).

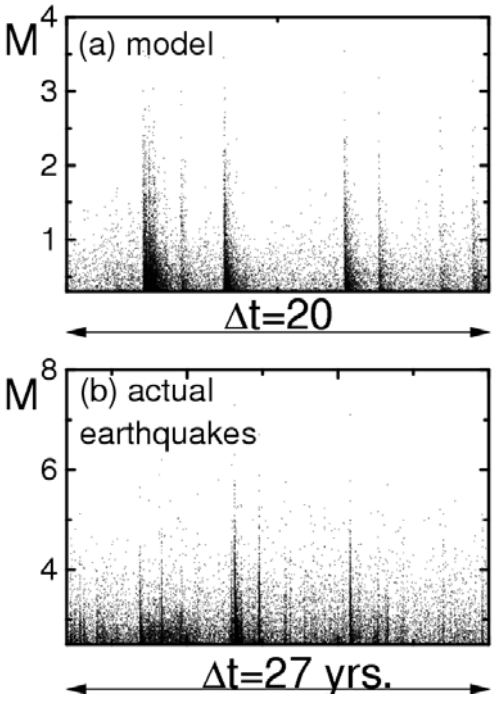

Figure 3. (a)Magnitude-time plot for a 200×200 system in the presence of relaxation ($k_1 = 0.005$, $k_0 = 0.1$, $\sigma_f = 0.8$, $\sigma_x = 0.8$, $R/V = 5$). (b) Actual earthquakes in the California area from years 1980-to-2008 [*NCDEC and ANSS*, 2008].

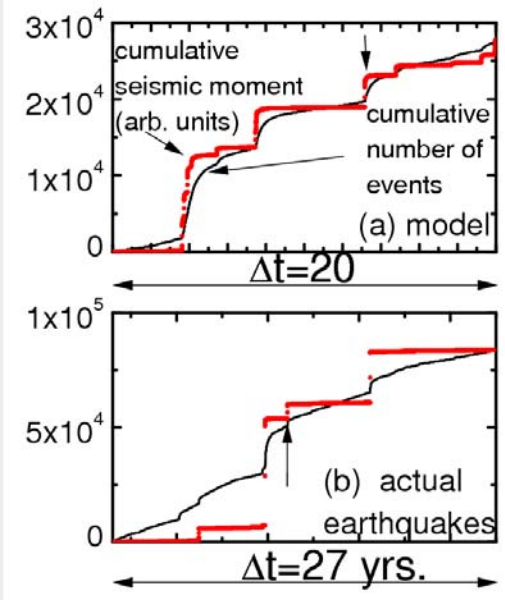

Figure 4. Cumulative number of events and cumulative seismic moment for the sequences presented in Fig. 3. The lower cutoff values of magnitude are $M_0 = 0.7$ for our data, and $M_0 = 2$ for the California data.

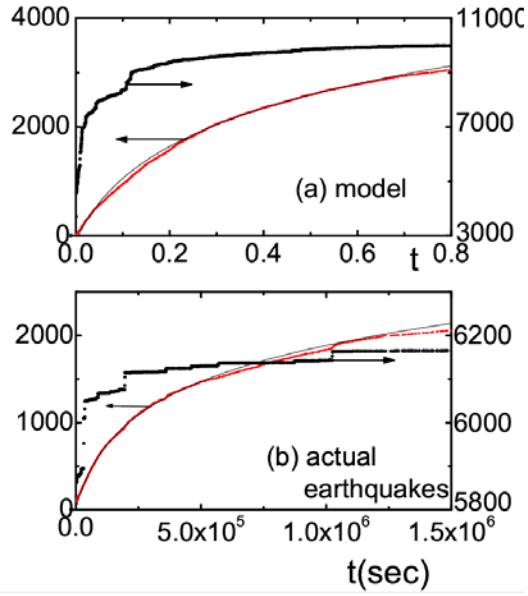

Figure 5. Detail to Fig. 4. Cumulative number of events and cumulative seismic moment (taken as zero just before the main shock), following the events indicated by vertical arrows in Fig. 4. In both cases, continuous lines correspond to a cumulative Omori law with $p = 1$.

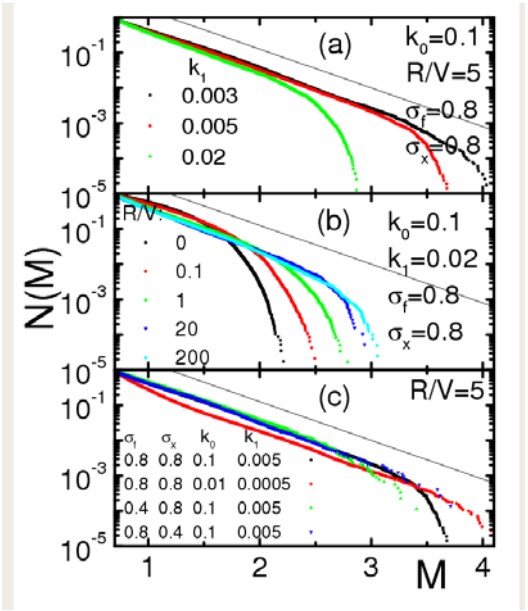

Figure 6. Building of a robust GR law in the presence of relaxation. (a) Dependence of the large size cutoff on the value of k_1. (b) Convergence of the decaying law to a well defined limit when increasing relaxation. (c) Independence of the results on other parameters of the model. In all cases the system size is large enough to avoid finite size effects for all set of parameters (sizes from 200×200 to 600×600 are used). Events with $M < 0.7$ are not displayed since spurious mesh dependences are expected in this range (see text).

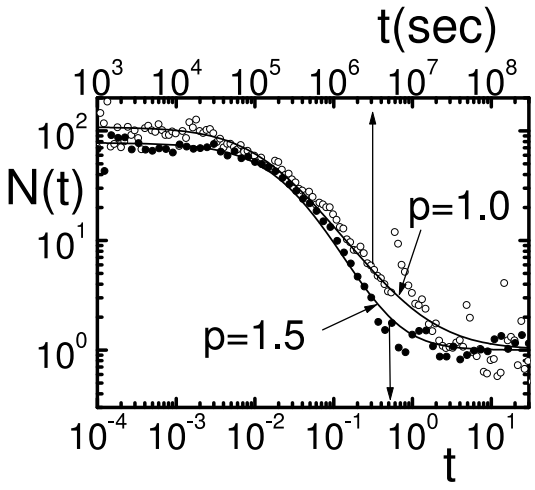

Figure 7. Number of events after main shocks in our model (full symbols) for parameters and system size as in Fig. 3a, normalized to the background seismicity (i.e., $N(t \to \infty) = 1$). We stacked the events after about 450 main shocks with $M > 3$, and the lower magnitude cut off used to count aftershocks is $M_0 = 1.5$. For comparison, the same analysis for data in the California region is presented with open symbols. In this case we sum over 7 events of magnitude larger than 6.0. For this case $M_0 = 2.0$. For reference, the continuous lines correspond to decays following the Omori law, with exponents $p = 1.0$, and $p = 1.5$.

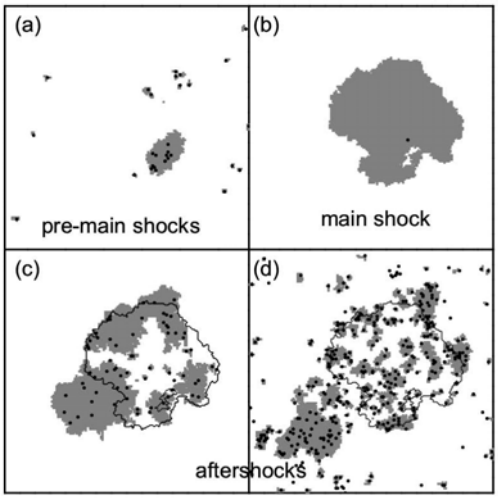

Figure 8. Distribution of events before and after a main shock. All panels depict the same portion of size 160×160 of a system with parameters as in Fig. 3a. In gray we show the portion of the system that has experienced slip in the corresponding time interval, and with small circles we indicate the epicenters of all independent events that contributed to this slip. Panel (a) shows the events in a time interval $\Delta t = 1$ before the main shock, which is depicted in panel (b). Panels (c) and (d) show respectively aftershocks in the time interval $\Delta t = 0.0177$ (c), and in a subsequent interval $\Delta t = 5$ (d) (the contour of the slip region of the main shock is highlighted for better comparison). Note the difference between the time intervals considered. Only events of magnitude larger than $M_0 = 0.7$ are considered.

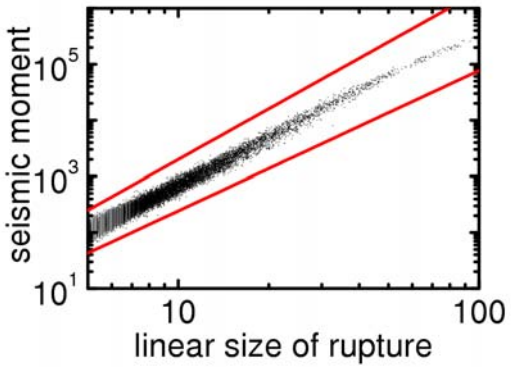

Figure 9. Seismic moment S as a function of square root of the number of blocks that participate in each earthquake. An almost univocous relation exists between these two quantities, that follows approximately a power law with an exponent between 2.5 and 3. The continuous lines have slopes 2.5, and 3, for reference (parameters as in Fig. 3a).

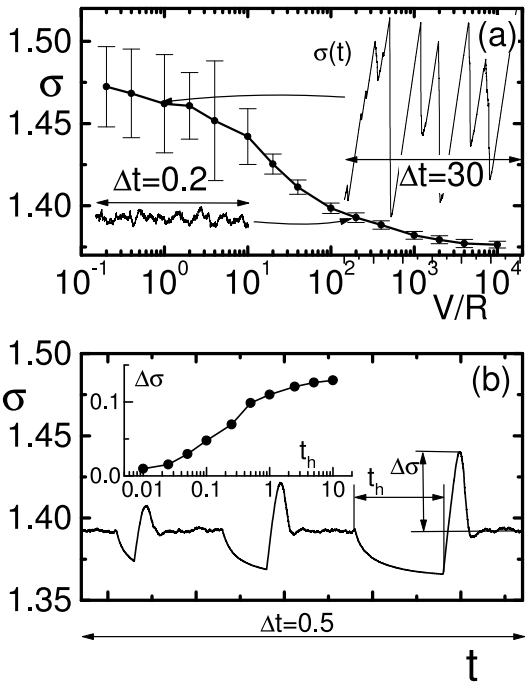

Figure 10. Frictional properties of the model. (a) Mean stress in a system of 200×200 as a function of relative velocity. Bars indicate the standard deviation of the data. A detail of the temporal dependence of stress is given for two points, emphasizing the larger fluctuations that appear when relative velocity is lower. (b) Time evolution of stress in a system in which velocity is changed from $V/R = 0$ in the hold periods, to $V/R = 200$ in the rest of time (results shown correspond to an average over ten realizations). Inset: The value of the stress peak is seen to increase logarithmically with the hold time.